New Accomplishments on the Equivalence of the First-Order Displacement-Based Zigzag Theories through a Unified Formulation

Journal of
Composites Science

MDPI

Article

New Accomplishments on the Equivalence of the First-Order Displacement-Based Zigzag Theories through a Unified Formulation

Marco Di Sciuva and Matteo Sorrenti *

Department of Mechanical and Aerospace Engineering, Politecnico di Torino, Corso Duca degli Abruzzi 24, 10129 Torino, Italy; marco.disciuva@formerfaculty.polito.it
* Correspondence: matteo.sorrenti@polito.it

Abstract: The paper presents a critical review and new accomplishments on the equivalence of the first-order displacement-based zigzag theories for laminated composite and sandwich structures. Zigzag theories (ZZTs) have widely spread among researchers over the last few decades thanks to their accuracy in predicting the response of multilayered composite and sandwich structures while retaining the simplicity of their underlying equivalent single-layer (ESL) theory. The displacement field consists of two main contributions: the global one, able to describe the overall structural behaviour, and the local layer-wise one that considers the transverse shear continuity at the layer interfaces that describe the "zigzag" displacement pattern typical of multilayered structures. In the framework of displacement-based linear ZZTs, various assumptions have been made on the local contribution, and different theories have been deduced. This paper aims to provide a unified formulation for first-order ZZTs, highlighting some common aspects and underlying equivalencies with existing formulations. The mathematical demonstrations and the numerical examples prove the equivalence of the approaches to characterising local zigzag enrichment. Finally, it is demonstrated that the kinematic assumptions are the discriminants of the ZZTs' accuracy.

Keywords: first-order zigzag theories; refined zigzag theory; lightweight structures; bending; composite materials; interlaminar continuity

Citation: Di Sciuva, M.; Sorrenti, M. New Accomplishments on the Equivalence of the First-Order Displacement-Based Zigzag Theories through a Unified Formulation. *J. Compos. Sci.* **2024**, *8*, 181. https://doi.org/10.3390/jcs8050181

Academic Editor: Francesco Tornabene

Received: 16 March 2024
Revised: 11 April 2024
Accepted: 9 May 2024
Published: 12 May 2024

1. Introduction

In the last few decades, laminated composite and sandwich structures have been extensively used in many engineering fields (e.g., aerospace, marine, energy, automotive, civil) due to their attractive mechanical properties, tailorability and high load-bearing capabilities compared to their low weight [1]. On the other hand, the combination of adjacent layers of different materials with different mechanical properties introduces a transverse anisotropy that must be addressed in the structural analysis to prevent some of the most common laminate failures, e.g., delamination and debonding. Therefore, an accurate and efficient mathematical model is necessary to provide a viable solution for engineering applications.

Clearly, the exact solution for the three-dimensional elasticity problem of general multilayered composites and sandwich structures is desirable. Historically, Pagano [2–4], Srinivas and Rao [5,6], Savoia and Reddy [7,8], and Noor and Burton [9,10] are some of the most referenced authors for the analytical three-dimensional analysis of laminated plates. Recently, the framework of available exact three-dimensional solutions has been enriched by Kashtalyan [11] for functionally graded (FG) rectangular plates and by Brischetto [12,13] for multilayered and FG plates and curved shells.

As reported in the abovementioned papers, the range of applicability of these solutions is limited to very specific lamination schemes, simply supported boundary conditions and

trigonometric distribution of load pressures, that are not representative of industrial applications. The finite element method (FEM), thanks to the solid elements, is an alternative approach able to reproduce an approximate solution for the governing equations of more complex problems. However, its greatest limitation is the prohibitive computational cost of addressing large, complex, multilayered structures.

Researchers' efforts during the last few decades focused on finding new, accurate and computationally efficient mathematical models for studying the response of multilayered structures. For instance, equivalent single-layer (ESL) theories assume a displacement field for the whole laminate thickness, which is a function of a limited number of kinematic unknowns. The widely acknowledged ESL theories are the classical plate theory (CPT) [14], the first-order shear deformation theory (FSDT) [15,16] and Reddy's third-order shear deformation theory (TSDT) [17]. These models are often accurate in predicting global quantities, such as maximum displacements, frequencies and buckling loads, and have been implemented in commercial finite element codes for their low computational cost. However, their kinematic assumptions result in an erroneous prediction of the real through-the-thickness distributions of in-plane displacements and transverse shear stresses which are fundamental in multilayered structures. In the open literature, other ESL models are available, and the interested reader is referred to the review of Abrate and Di Sciuva [18] for a more exhaustive overview.

On the other hand, layer-wise (LW) models assume an independent displacement field governed by an arbitrary number of kinematic variables for each layer. By enforcing the continuity displacement requirements at the interfaces, the resulting LW models are more accurate than the ESL ones compared to the three-dimensional elasticity response. It is easy to see that the LW models are more computationally expensive than the ESL counterparts due to the number of kinematic variables' dependency on the number of layers. For the sake of conciseness, more details on the current LW model available in the literature are reported in Refs. [19,20].

In the late 1980s, a new class of theories, i.e., zigzag theories (ZZTs), was introduced to overcome the computational limitations of LW theories and the lack of accuracy in ESL models. Firstly introduced by Di Sciuva [21], the basic assumption of a ZZT is the superposition of two main contributions in the displacement field: a global one able to reproduce the general plate behaviour involving only a few kinematic variables, and a local layer-wise displacement refinement capable of capturing the changes in the material properties across the laminate thickness. Generally, the local displacement refinements are given by some appropriate functions of thickness coordinate, i.e., the "*zigzag functions*", and multiplied by proper unknown kinematic variables. The zigzag functions are commonly formulated to ensure the transverse shear continuity at the layer interfaces, also known as "*interlaminar continuity*". These assumptions represent the major advantages of ZZTs, i.e., greater accuracy, similar to that achieved by LW models, while retaining simplicity, providing few kinematic unknowns and computational attractiveness.

Various authors have proposed different methodologies for defining the zigzag local contribution. In Di Sciuva's [22,23], Cho and Parmerter's [24,25] and Icardi's [26–28] works, the changes in slopes in the local displacement refinement have been ensured by the Heaviside step functions, whereas the null value of zigzag contribution and the transverse shear strain of the reference layer are used to characterise the zigzag function. In the aforementioned models, the number of kinematic variables is the same as that of FSDT, but to formulate suitable finite elements, C^1-continuity is required for shape function selection (less attractive from a computational point of view) since the derivatives of the transverse displacement appear in the global contribution of the in-plane displacements. Additionally, some inconsistencies arise when these models try to address problems with clamped boundary conditions, i.e., null transverse shear stress resultants, as reported in Ref. [29].

In Averill's zigzag model [30,31], a first attempt to overcome the previous limitation has been made by introducing a new kinematic variable and enforcing the continuity

condition of the transverse shear stress across the laminate through a penalisation term in the governing functional. In Murakami's approach [32], the proposed zigzag functions are not based on the transverse shear stress continuity, and their distribution is assumed a priori known and not dependent on the geometry or mechanical material properties.

The refined zigzag theory (RZT), formulated by Tessler et al. [29,33], has been proposed to overcome the difficulties and inconsistencies of Di Sciuva's and Averill's models. As in Averill's model, the kinematics of RZT involve an additional kinematic unknown for displacement refinement (e.g., four kinematic variables for beams and seven for plates). The typical constant distributions of the transverse shear stresses seen in Di Sciuva's ZZT are avoided by ensuring only a partial transverse shear stress continuity at the layer interfaces. Moreover, two vanishing conditions on the displacement refinements are required on the top and bottom external surfaces before the zigzag functions are defined. The RZT approach has been shown to accurately predict global quantities (e.g., displacements, natural frequencies and buckling loads) and local through-the-thickness distributions for displacements, strains and stresses. The kinematics requires only C^0-continuity for the selection of shape functions, and efficient low-order finite elements can be formulated. The partial enforcement of the transverse shear stress has been demonstrated to achieve a more realistic representation of the shear deformability without the adoption of any shear correction factor.

With the adoption of the same kinematics and procedure of the RZT in defining the zigzag functions, the zigzag contribution has been enriched by Sorrenti and Di Sciuva [34] to analyse the behaviour of general plates in which the lamination scheme (e.g., symmetric and antisymmetric angle-ply) introduces a transverse shear anisotropy. The enhanced refined zigzag theory (en-RZT) accurately predicts the structural response for these particular lamination schemes and can obtain the same results as the standard RZT. In this sense, the en-RZT can be seen as a generalisation of the RZT.

The aforementioned zigzag models have been widely addressed in the literature. For instance, Massabò and co-workers have investigated the presence of lamination defects and damages in beam/plate structures [35–38] using a similar procedure originally developed by Di Sciuva's ZZT. Based on Cho and Parmerter's model, Nguyen et al. [39,40] addressed the viscoelastic study of laminated composite plates. In the RZT-based framework, various problems and study cases have been addressed, including functionally graded and carbon-nanotube-reinforced structures [41–43], the transient response of innovative multilayered plates [44,45], delamination and damage assessment [46–50], thermal and buckling load conditions [51,52], linear and non-linear analyses [53–55], laminated shell problems [56–58], angle-ply lamination schemes [59–61], laminates with viscoelastic layers [62,63], solutions using the peridynamic differential operator [64,65], optimisation [66], isogeometric analysis (IGA) [67,68] and inverse FEM studies [69–73] for structural health monitoring purposes.

Hence, there is a clear interest in the scientific community in adopting and adapting existing zigzag models for various engineering applications.

However, it seems crucial to better clarify the fundamental aspects characterising the formulation of zigzag models, emphasising the different roles covered by the kinematic assumptions and the approaches to characterising the local displacement contribution.

This paper aims to present a unified formulation for displacement-based first-order zigzag theories, starting from a general expression for the displacement field. Then, the transverse shear stress continuity conditions are reformulated in order to highlight the contributions given by the global and local displacements. Subsequently, three different scenarios are presented to characterise and express the local displacement contribution in a recursive formulation. The general ZZTs governing equations and variationally consistent boundary conditions are obtained using the d'Alembert principle and solved analytically for some case studies. The numerical assessments substantiate the general equivalence considerations achieved in the unified model formulation; i.e., the constraints on the local displacement contributions to characterising the through-the-thickness zigzag distributions are not a discriminant of the theory's accuracy.

2. Mathematical Formulation of Generalised Displacement-Based First-Order Zigzag Theories

2.1. Geometrical Preliminaries for Plates

We consider a multilayered flat plate made of a finite number N of perfectly bonded layers, as shown in Figure 1. V is the plate's volume, and h is its total thickness. The points of the plate are referred to an orthogonal Cartesian coordinate system defined by the vector $\mathbf{X} = \{x_i\}$ $(i = 1, 2, 3)$, where the vector $\mathbf{x} = \{x_\alpha\}$ $(\alpha = 1, 2)$ represents the set of the in-plane coordinates on the reference plane, here chosen to be the midplane of the plate denoted with Ω, as represented in Figure 1. Let x_3 be the coordinate normal to the reference plane, see Figure 1b, so that $x_3 \in [z_B, z_T]$, and $z_M = \frac{1}{2}(z_B + z_T)$ is the transverse coordinate of the midplane of the plate.

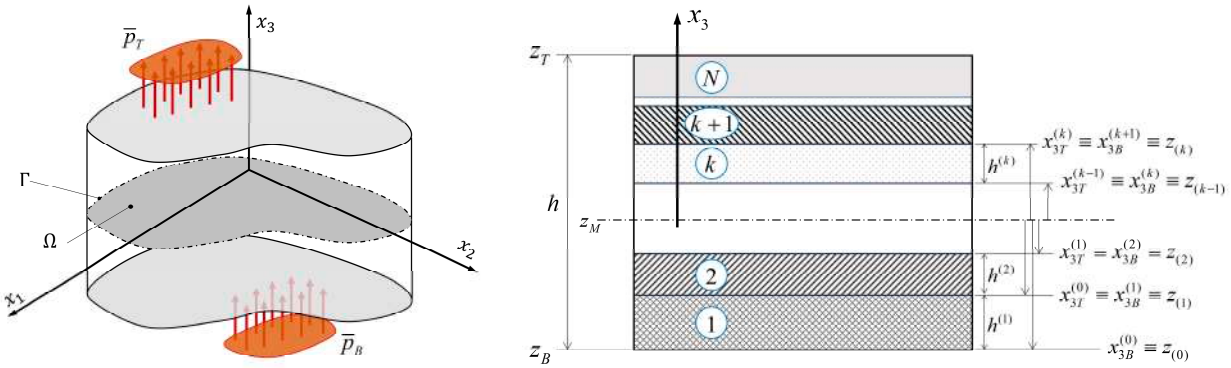

(**a**) (**b**)

Figure 1. General plate notation: (**a**) loads and coordinate reference system, (**b**) layer numbering and interface locations.

Let us define $S = S_u \cup S_\sigma$, the total cylindrical edge surface composed of S_u and S_σ, the portions on which the displacements and tractions are prescribed, respectively. Moreover, let $\overline{p}_B$ and $\overline{p}_T$ be the prescribed transverse pressure acting on the plate's bottom (B) and top (T) external surfaces, respectively. As denoted in Figure 1a, the contour line Γ of the reference surface Ω is the set of the plate points given by the intersection of the cylindrical edge surface, i.e., $\Gamma = S \cap \Omega = \Gamma_u \cup \Gamma_\sigma$ $(\Gamma_u \cap \Gamma_\sigma = \varnothing)$, with $\Gamma_u = S_u \cap \Omega$ and $\Gamma_\sigma = S_\sigma \cap \Omega$.

According to Figure 1, let us denote the quantities corresponding to the kth layer with the superscript $(\cdot)^{(k)}$ $(k = 1, 2, \ldots, N)$ and the quantities evaluated at the kth interface with the subscript $(\cdot)_{(k)}$ $(k = 1, 2, \ldots, N-1)$, i.e., between the kth and the $(k+1)$th layers, so that $z_{(k)} = x_{3T}^{(k)} = x_{3B}^{(k+1)}$. Moreover, $z_{(0)}$ and $z_{(N)}$ denote the thickness-wise coordinates of the bounding bottom and top surfaces of the whole plate.

The quantities denoted with the subscript B are those corresponding to the bottom of the plate/layer, the quantities denoted with the subscript T are those at the top of the plate/layer and the quantities denoted with M are those corresponding to the midplane of the plate/layer. For simplicity, the thickness of each layer and the whole plate are assumed to be constant.

For further convenience, let us introduce a local coordinate system $\left(\mathbf{x}, x_3^{(k)}\right)$ for each kth layer; its origin, located on its midplane, $z_M^{(k)} = \frac{1}{2}\left(z_B^{(k)} + z_T^{(k)}\right)$ coordinate (see Figure 2), implies

$$x_3^{(k)} \in \left[x_{3B}^{(k)}, x_{3T}^{(k)}\right] \equiv \left[z_{(k-1)}, z_{(k)}\right] \tag{1}$$

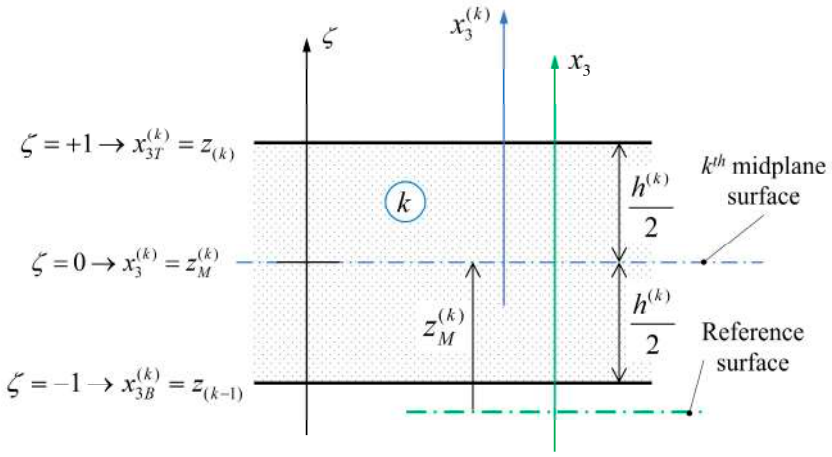

Figure 2. General layer notation: geometrical quantities and local-layer reference frame.

Let us introduce the non-dimensional transverse coordinate $\zeta \in [-1, +1]$; the following relation holds:

$$x_3^{(k)} = z_B^{(k)} L_B(\zeta) + z_T^{(k)} L_T(\zeta) = \frac{1}{2}\left(z_B^{(k)} + z_T^{(k)}\right) + \frac{1}{2}\left(z_T^{(k)} - z_B^{(k)}\right)\zeta = z_M^{(k)} + \frac{h^{(k)}}{2}\zeta \quad (2)$$

where

$$L_B(\zeta) = \frac{1}{2}(1-\zeta); L_T(\zeta) = \frac{1}{2}(1+\zeta) \quad -1 \leq \zeta \leq +1 \quad (3)$$

are the linear Lagrangian interpolation polynomials.

From Equation (2),

$$\zeta = \frac{2}{h^{(k)}}\left(x_3^{(k)} - z_M^{(k)}\right) \quad (4)$$

Note that Equations (2) and (4) also apply to the whole plate. Omitting the superscript (k) in Equation (2) yields

$$x_3 = z_B L_B(\zeta) + z_T L_T(\zeta) = z_M + \frac{h}{2}\zeta \quad (5)$$

The material of each layer is assumed to be elastic orthotropic with a plane of elastic symmetry parallel to the reference surface. Moreover, its principal orthotropy directions are arbitrarily oriented with respect to the in-plane reference frame with an angle denoted with $Y^{(k)}$, measured counterclockwise from the positive x_3-axis.

Furthermore, the symbol $(\cdot)_{,i}$ refers to the derivative of the function $(\cdot)$ with respect to the coordinate x_i, i.e., $(\cdot)_{,i} = \frac{\partial(\cdot)}{\partial x_i}$. The prescribed quantities are denoted with an overbar. The Einstein summation convention over repeated indices is adopted, with Latin indices ranging from 1 to 3 and Greek indices ranging from 1 to 2.

2.2. Interlaminar Continuity Conditions

Let us denote with $\mathbf{U}(\mathbf{X}) = \{\widetilde{u}_i\}(i = 1, 2, 3)$ the displacement vector of a point belonging to the plate, defined according to its orthogonal Cartesian components. Assuming the linear strain–displacement relations, the infinitesimal strain tensor in engineering notation is as follows:

$$\begin{gathered} \varepsilon_{11} = \frac{\partial \widetilde{u}_1}{\partial x_1}; \ \varepsilon_{22} = \frac{\partial \widetilde{u}_2}{\partial x_2}; \ \varepsilon_{33} = \frac{\partial \widetilde{u}_3}{\partial x_3}; \\ \gamma_{12} = \frac{\partial \widetilde{u}_1}{\partial x_2} + \frac{\partial \widetilde{u}_2}{\partial x_1}; \ \gamma_{13} = \frac{\partial \widetilde{u}_1}{\partial x_3} + \frac{\partial \widetilde{u}_3}{\partial x_1}; \\ \gamma_{23} = \frac{\partial \widetilde{u}_2}{\partial x_3} + \frac{\partial \widetilde{u}_3}{\partial x_2} \end{gathered} \quad (6)$$

Taking into account that the material is linearly elastic and orthotropic, the generalised Hooke's law is written as follows:

$$\begin{Bmatrix} \boldsymbol{\sigma} \\ \boldsymbol{\tau} \end{Bmatrix} = \mathbf{C} \begin{Bmatrix} \boldsymbol{\varepsilon} \\ \boldsymbol{\gamma} \end{Bmatrix} \tag{7}$$

where $\boldsymbol{\sigma}^T = \begin{bmatrix} \sigma_{11} & \sigma_{22} & \sigma_{33} \end{bmatrix}$, $\boldsymbol{\tau}^T = \begin{bmatrix} \tau_{12} & \tau_{13} & \tau_{23} \end{bmatrix}$ are the sub-vectors defining the normal and shear stresses, respectively. Moreover, $\boldsymbol{\varepsilon}^T = \begin{bmatrix} \varepsilon_{11} & \varepsilon_{22} & \varepsilon_{33} \end{bmatrix}$ and $\boldsymbol{\gamma}^T = \begin{bmatrix} \gamma_{12} & \gamma_{13} & \gamma_{23} \end{bmatrix}$ are the sub-vectors defining the normal axial-transverse and shear strains, respectively. The matrix $\mathbf{C}$ represents the stiffness tensor written according to the Voigt–Kelvin notation [74] that contains the components of the elastic material properties.

From the three-dimensional elasticity theory, displacements and stresses must satisfy the *interlaminar continuities* between two perfectly bonded layers and the traction conditions on the top and bottom external surfaces:

(i) Continuity of the displacement field (geometric)

$$\widetilde{u}_i^{(k)}\left(\mathbf{x}, z_T^{(k)}\right) = \widetilde{u}_i^{(k+1)}\left(\mathbf{x}, z_B^{(k+1)}\right) \quad (k = 1, \ldots, N-1) \tag{8}$$

(ii) Continuity of the transverse shear and normal stresses, and continuity of the gradient of the transverse normal stress (static)

$$\boldsymbol{\sigma}_t^{(k)}\left(\mathbf{x}, z_T^{(k)}\right) = \boldsymbol{\sigma}_t^{(k+1)}\left(\mathbf{x}, z_B^{(k+1)}\right) \quad (k = 1, \ldots, N-1) \tag{9}$$

$$\begin{matrix} \sigma_{33}^{(k)}\left(\mathbf{x}, z_T^{(k)}\right) = \sigma_{33}^{(k+1)}\left(\mathbf{x}, z_B^{(k+1)}\right) \\ \sigma_{33,3}^{(k)}\left(\mathbf{x}, z_T^{(k)}\right) = \sigma_{33,3}^{(k+1)}\left(\mathbf{x}, z_B^{(k+1)}\right) \end{matrix} \quad (k = 1, \ldots, N-1) \tag{10}$$

where $\boldsymbol{\sigma}_t^T = \begin{bmatrix} \tau_{13} & \tau_{23} \end{bmatrix}$.

Since the bottom and top external surfaces of the laminated plate are loaded with only pressure, see Figure 1a, the following traction conditions must be satisfied:

(i) Traction-free condition on the transverse shear stresses

$$\boldsymbol{\sigma}_t^{(1)}\left(\mathbf{x}, z_B^{(1)}\right) = \boldsymbol{\sigma}_t^{(N)}\left(\mathbf{x}, z_T^{(N)}\right) = \mathbf{0} \tag{11}$$

(ii) Traction condition on transverse normal stress and its gradient

$$\begin{matrix} \sigma_{33}^{(1)}\left(\mathbf{x}, z_B^{(1)}\right) = \overline{p}_B(\mathbf{x}); \ \sigma_{33}^{(N)}\left(\mathbf{x}, z_T^{(N)}\right) = \overline{p}_T(\mathbf{x}) \\ \sigma_{33,3}^{(1)}\left(\mathbf{x}, z_B^{(1)}\right) = \sigma_{33,3}^{(N)}\left(\mathbf{x}, z_T^{(N)}\right) = 0 \end{matrix} \tag{12}$$

2.3. Equivalent Single Layer (ESL) Theories

As a final preliminary consideration, it is worth spending some more words on the kinematics of ESL models. Clearly, the expression for $\widetilde{u}_i(\mathbf{x}, x_3; t)$ differs on the kinematic assumptions; however, the ESL theories generally assume a power series expansion of the thickness coordinate. Across the whole paper, this contribution is named *global* (G), and a general expression reads

$$\widetilde{u}_i(\mathbf{X}; t) = \widetilde{u}_i^G(\mathbf{x}, x_3; t) = Z_i^{(r)}(x_3) u_i^{G(r)}(\mathbf{x}; t) \tag{13}$$

where $\widetilde{u}_i^G(\mathbf{x}, x_3; t)$ is the global contribution of the displacement along the ith axis, $u_i^{G(r)}(\mathbf{x}; t)$ are the unknown generalised displacements of the series expansion and $Z_i^{(r)}(x_3)$ are the set

of a priori assumed linearly independent functions of the series expansion from Ref. [75]. This last term is generally assumed to be a power series expansion of x_3,

$$Z_i^{(r)}(x_3) = x_3^r (r = 1, 2, \ldots, R) \tag{14}$$

The orthogonal set of polynomial functions given by Equation (14) corresponds to Legendre's polynomial of the first kind. Other choices are admissible and can be found in the open literature (see, for instance, Ref. [18]). Notably, the kinematics along the thickness-wise direction is assumed to be at least C^1-continuous and independent from the laminate lay-up. Thus, an equivalent anisotropic single-layer plate model can easily replace the multilayered structure. Note that most of the polynomial theories assume $R_1 = R_2 > R_3$, where typically $R_3 = 0$.

2.4. First-Order Zigzag Theories, Strain and Stress Definitions

As usual in the displacement-based theories for plates and shells, the through-the-thickness distribution of the displacement field is assumed a priori. According to the approach commonly adopted for zigzag theories, the in-plane kinematics is based on the superposition of a global (G) contribution (which is continuous across the laminate thickness, as defined earlier) and a local (L) layer-wise correction. The local displacement contribution is assumed to be piecewise linear (C^0-continuous) with jumps in the first derivatives at the interfaces between adjacent layers. By neglecting the transverse normal deformability, i.e., $\varepsilon_{33} = \widetilde{u}_{3,3} = 0$, the transverse deflection is assumed to be uniform along the thickness directions. Thus, we can write

$$\begin{aligned} \tilde{\mathbf{u}}^{(k)}(\mathbf{x}, x_3; t) &= \tilde{\mathbf{u}}^{G}(\mathbf{x}, x_3; t) + \tilde{\mathbf{u}}^{L(k)}(\mathbf{x}, x_3; t) \ (k = 1, \ldots, N) \\ \widetilde{u}_3^{(k)}(\mathbf{x}, x_3; t) &= u_3^{(0)}(\mathbf{x}; t) \end{aligned} \tag{15}$$

In Equation (15), it is assumed that the global contribution is given by the FSDT, i.e.,

$$\tilde{\mathbf{u}}^{G}(\mathbf{x}, x_3; t) = \mathbf{u}^{(0)}(\mathbf{x}; t) + x_3 \boldsymbol{\theta}(\mathbf{x}; t) \tag{16}$$

where $\mathbf{u}^{(0)T} = \begin{bmatrix} u_1^{(0)} & u_2^{(0)} \end{bmatrix}$ is the uniform part of the in-plane displacements and $u_3^{(0)}$ the transverse one; $\boldsymbol{\theta}^T = \begin{bmatrix} \theta_1 & \theta_2 \end{bmatrix}$ represents the average bending rotations around the positive direction of x_2 and the negative direction of x_1.

Moreover,

$$\tilde{\mathbf{u}}^{L(k)}(\mathbf{x}, x_3; t) = \mathbf{u}_B^{L(k)}(\mathbf{x}; t) L_B(\zeta) + \mathbf{u}_T^{L(k)}(\mathbf{x}; t) L_T(\zeta) \tag{17}$$

Similarly, the global contribution given by Equation (16) can be rewritten in terms of the bottom and top plate in-plane displacements, i.e.,

$$\tilde{\mathbf{u}}^{G(k)}(\mathbf{X}; t) = \mathbf{u}^{(0)}(\mathbf{x}; t) + x_3 \boldsymbol{\theta}(\mathbf{x}; t) = \mathbf{u}_B^{G}(\mathbf{x}; t) L_B(\zeta) + \mathbf{u}_T^{G}(\mathbf{x}; t) L_T(\zeta) \tag{18}$$

Using the previous relations yields

$$\begin{aligned} \mathbf{u}^{(0)}(\mathbf{x}; t) &= \frac{\mathbf{u}_T^G(\mathbf{x};t) + \mathbf{u}_B^G(\mathbf{x};t)}{2} + z_M \frac{\mathbf{u}_T^G(\mathbf{x};t) - \mathbf{u}_B^G(\mathbf{x};t)}{h} \\ \boldsymbol{\theta}(\mathbf{x}; t) &= \frac{\mathbf{u}_T^G(\mathbf{x};t) - \mathbf{u}_B^G(\mathbf{x};t)}{h} \end{aligned} \tag{19}$$

The local contribution to the in-plane kinematics given by Equation (17) adds $4N$ unknown in-plane generalised displacements. For each kth layer, we have two bottom, i.e., $\mathbf{u}_B^{L(k)}(\mathbf{x}; t)$, and two top, i.e., $\mathbf{u}_T^{L(k)}(\mathbf{x}; t)$, unknown in-plane generalised displacements. The number of these variables can be reduced by enforcing an appropriate set of constraint conditions.

Neglecting the transverse normal stress, i.e., $\sigma_{33} = 0$, according to the theory of elasticity, the in-plane displacements and the transverse shear stresses must satisfy the continuity conditions at the $N-1$ interfaces; see Equations (8) and (9).

As the global contribution satisfies the in-plane displacement continuity conditions at the interfaces, the constraint given by Equation (8) implies that

$$\mathbf{u}_T^{L(k)} = \mathbf{u}_B^{L(k+1)} = \mathbf{u}_{(k)}^{L} \ (k = 1, \ldots, N-1) \tag{20}$$

whereas $\mathbf{u}_{(0)}^{L}$ and $\mathbf{u}_{(N)}^{L}$ are, respectively, the bottom and top plate surface local displacements.

Thus, from the continuity conditions on the displacements (that introduce $2(N-1)$ constraints) and on the transverse shear stresses (that add further $2(N-1)$ constraint conditions), four free unknown local contributions to the in-plane generalised displacements result. The following section discusses three different scenarios to determine the remaining four unknowns.

Consistent with linear strain–displacement relations and using the two-dimensional *del operator* $\nabla(\cdot)^T = \lfloor (\cdot)_{,1} \quad (\cdot)_{,2} \rfloor$, we define the strain components as

$$\begin{aligned} \tilde{\boldsymbol{\varepsilon}}_p^{(k)}(\mathbf{X};t) &= \left\{ \begin{array}{c} \widetilde{u}_{1,1}^{(k)} \\ \widetilde{u}_{1,2}^{(k)} \\ \widetilde{u}_{2,1}^{(k)} \\ \widetilde{u}_{2,2}^{(k)} \end{array} \right\} = \left\{ \begin{array}{c} \nabla \widetilde{u}_1^{(k)} \\ \nabla \widetilde{u}_2^{(k)} \end{array} \right\} = \left\{ \begin{array}{c} \tilde{\mathbf{E}}_{p1}^{(k)} \\ \tilde{\mathbf{E}}_{p2}^{(k)} \end{array} \right\} \\ \tilde{\boldsymbol{\gamma}}^{(k)}(\mathbf{X};t) &= \left\{ \begin{array}{c} \widetilde{\gamma}_{13}^{(k)} \\ \widetilde{\gamma}_{23}^{(k)} \end{array} \right\} = \left\{ \begin{array}{c} \widetilde{u}_{1,3}^{(k)} + \widetilde{u}_{3,1}^{(k)} \\ \widetilde{u}_{2,3}^{(k)} + \widetilde{u}_{3,2}^{(k)} \end{array} \right\} = \tilde{\mathbf{u}}_{,3}^{(k)} + \nabla \widetilde{u}_3^{(k)} \end{aligned} \tag{21}$$

Correspondingly, the linear elastic constitutive relations read

$$\begin{aligned} \tilde{\boldsymbol{\sigma}}_p^{(k)}(\mathbf{X};t) &= \left\{ \begin{array}{c} \sigma_{11}^{(k)} \\ \sigma_{12}^{(k)} \\ \sigma_{21}^{(k)} \\ \sigma_{22}^{(k)} \end{array} \right\} = \left\{ \begin{array}{c} \tilde{\boldsymbol{\sigma}}_{p1}^{(k)} \\ \tilde{\boldsymbol{\sigma}}_{p2}^{(k)} \end{array} \right\} = \overline{\mathbf{Q}}_p^{(k)} \tilde{\mathbf{E}}_p^{(k)}(\mathbf{X};t); \\ & \qquad\qquad (k = 1, \ldots, N) \\ \tilde{\boldsymbol{\sigma}}_t^{(k)}(\mathbf{X};t) &= \left\{ \begin{array}{c} \tau_{13}^{(k)} \\ \tau_{23}^{(k)} \end{array} \right\} = \overline{\mathbf{Q}}_t^{(k)} \tilde{\boldsymbol{\gamma}}^{(k)}(\mathbf{X};t) \end{aligned} \tag{22}$$

where $\tilde{\boldsymbol{\sigma}}_p^{(k)}$ are the in-plane stress components and $\tilde{\boldsymbol{\sigma}}_t^{(k)}$ the transverse shear stress ones. Moreover, in Equation (22), $\overline{\mathbf{Q}}_p^{(k)}$ and $\overline{\mathbf{Q}}_t^{(k)}$ are, respectively, the in-plane reduced and transverse shear elastic stiffness coefficients of the kth layer, expressed in the reference coordinate system [76]. They read

$$\begin{aligned} \overline{\mathbf{Q}}_p^{(k)} &= \left[\begin{array}{cccc} \overline{Q}_{11} & \overline{Q}_{16} & \overline{Q}_{16} & \overline{Q}_{12} \\ \overline{Q}_{16} & \overline{Q}_{66} & \overline{Q}_{66} & \overline{Q}_{26} \\ \overline{Q}_{16} & \overline{Q}_{66} & \overline{Q}_{66} & \overline{Q}_{26} \\ \overline{Q}_{12} & \overline{Q}_{26} & \overline{Q}_{26} & \overline{Q}_{22} \end{array} \right]^{(k)} = \left[\begin{array}{cc} \overline{\mathbf{Q}}_{p11}^{(k)} & \overline{\mathbf{Q}}_{p12}^{(k)} \\ \overline{\mathbf{Q}}_{p12}^{(k)T} & \overline{\mathbf{Q}}_{p22}^{(k)} \end{array} \right] \\ \overline{\mathbf{Q}}_t^{(k)} &= \left[\begin{array}{cc} \overline{Q}_{44} & \overline{Q}_{45} \\ \overline{Q}_{45} & \overline{Q}_{55} \end{array} \right]^{(k)} \end{aligned} \tag{23}$$

2.5. Transverse Shear Strain Considerations

The transverse shear strain given by Equation (21) can be written highlighting the global and local contributions as follows:

$$\tilde{\boldsymbol{\gamma}}^{(k)}(\mathbf{X};t) = \tilde{\boldsymbol{\gamma}}^{G(k)}(\mathbf{X};t) + \tilde{\boldsymbol{\gamma}}^{L(k)}(\mathbf{X};t) (k = 1, \ldots, N) \tag{24}$$

where

$$\tilde{\boldsymbol{\gamma}}^{G(k)} = \begin{Bmatrix} \widetilde{\gamma}^G_{13} \\ \widetilde{\gamma}^G_{23} \end{Bmatrix} = \begin{Bmatrix} \widetilde{u}^G_{1,3} + u^{(0)}_{3,1} \\ \widetilde{u}^G_{2,3} + u^{(0)}_{3,2} \end{Bmatrix} = \begin{Bmatrix} \theta_1 + u^{(0)}_{3,1} \\ \theta_2 + u^{(0)}_{3,2} \end{Bmatrix} = \boldsymbol{\theta} + \nabla u^{(0)}_3 = \boldsymbol{\gamma}^G_{(0)} \tag{25}$$

$$\tilde{\boldsymbol{\gamma}}^{L(k)} = \mathbf{u}^{L(k)}_{,3} = \mathbf{u}^{L(k)} L_{B,3} + \mathbf{u}^{L(k+1)} L_{T,3} \tag{26}$$

Note that in Equation (25) and in Equation (26) (see Equation (2)),

$$L_{(B/T),3} = L_{(B/T),\zeta} \zeta_{,3} = \frac{2}{h^{(k)}} L_{(B/T),\zeta} = (-/+) \frac{1}{h^{(k)}} \tag{27}$$

Thus, Equations (25) and (26) read

$$\boldsymbol{\gamma}^G_{(0)} = \left(\mathbf{u}^G_B L_{B,\zeta} + \mathbf{u}^G_T L_{T,\zeta} \right) = \frac{1}{h} \left(\mathbf{u}^G_T - \mathbf{u}^G_B \right) + \nabla u^{(0)}_3 = \boldsymbol{\theta} + \nabla u^{(0)}_3 \tag{28}$$

$$\boldsymbol{\gamma}^{L(k)} = \left(\mathbf{u}^{L(k)}_B L_{B,\zeta} + \mathbf{u}^{L(k)}_T L_{T,\zeta} \right) \frac{2}{h^{(k)}} = \frac{1}{h^{(k)}} \left(\mathbf{u}^{L(k)}_T - \mathbf{u}^{L(k)}_B \right) = \boldsymbol{\theta}^{L(k)} \tag{29}$$

So, from Equation (29), the local top in-plane displacements of the kth layer read

$$\mathbf{u}^{L(k)}_T = h^{(k)} \boldsymbol{\gamma}^{L(k)} + \mathbf{u}^{L(k)}_B = \sum_{p=1}^{k} h^{(p)} \boldsymbol{\gamma}^{L(p)} + \mathbf{u}^{L(1)}_B \; (k = 1, \ldots, N) \tag{30}$$

Adopting the notation given in Equation (20),

$$\mathbf{u}^L_{(k)} = h^{(k)} \boldsymbol{\gamma}^{L(k)} + \mathbf{u}^L_{(k-1)} = \sum_{p=1}^{k} h^{(p)} \boldsymbol{\gamma}^{L(p)} + \mathbf{u}^L_{(0)} = \sum_{p=1}^{k} h^{(p)} \boldsymbol{\theta}^{L(p)} + \mathbf{u}^L_{(0)} \;\; (k = 1, \ldots, N) \tag{31}$$

As obtained in Equation (31), the local contribution to the interfacial in-plane displacements is expressed in terms of the local rotations $\boldsymbol{\theta}^{L(p)}$ and $\mathbf{u}^L_{(0)}$.

Comparing Equation (29) with the bending rotation given in Equation (19), the local contribution to the transverse shear strain gives the local contribution to the slope of the normal to the reference surface, i.e., $\boldsymbol{\gamma}^{L(k)} \equiv \boldsymbol{\theta}^{L(k)}$.

Note that from Equation (31), it follows that

$$\mathbf{u}^L_{(N)} - \mathbf{u}^L_{(0)} = \sum_{p=1}^{N} h^{(p)} \boldsymbol{\gamma}^{L(p)} = \sum_{p=1}^{N} h^{(p)} \boldsymbol{\theta}^{L(p)} \tag{32}$$

More specifically, Equation (32) highlights that if we require the mean value of the local contribution to the transverse shear strain to be zero, then the through-the-thickness integral of the local contribution (which is a piece-wise constant function) vanishes identically, i.e.,

$$\mathbf{u}^L_{(N)} - \mathbf{u}^L_{(0)} = \sum_{p=1}^{N} h^{(p)} \boldsymbol{\gamma}^{L(p)} = \int_{z_B}^{z_T} \boldsymbol{\gamma}^{L(p)} dz = \int_{z_B}^{z_T} \boldsymbol{\theta}^{L(p)} dz = \mathbf{0} \tag{33}$$

Alternatively, if we use Equation (33) as a constraint to be satisfied by the local contribution, the mean value of the local contribution to the transverse shear strain must be zero. In other terms, the mean value of the rotation of the normal is equal to the value given by the global contribution, i.e., $\boldsymbol{\theta}$.

2.6. Transverse Shear Stress Continuity

This section addresses the continuity condition of transverse shear stresses at the layer interfaces.

Recalling the continuity stress conditions expressed by Equation (9) and using the constitutive material relations, i.e., Equation (22), yields (it should be noted that the as-

sumed kinematics only allows a uniform thickness-wise distribution of the transverse shear stresses)

$$\overline{\mathbf{Q}}_t^{(k)}\left(\boldsymbol{\gamma}_{(0)}^G+\boldsymbol{\gamma}^{L(k)}\right)=\overline{\mathbf{Q}}_t^{(k+1)}\left(\boldsymbol{\gamma}_{(0)}^G+\boldsymbol{\gamma}^{L(k+1)}\right) \tag{34}$$

Elaborating further on Equation (34), it follows that

$$\begin{aligned}\boldsymbol{\gamma}^{L(k+1)} &= \overline{\mathbf{S}}_t^{(k+1)}\overline{\mathbf{Q}}_t^{(k)}\boldsymbol{\gamma}^{L(k)}+\mathbf{A}^{(k+1,k)}\boldsymbol{\gamma}_{(0)}^G\\ &= \left(\mathbf{I}+\mathbf{A}^{(k+1,k)}\right)\boldsymbol{\gamma}^{L(k)}+\mathbf{A}^{(k+1,k)}\boldsymbol{\gamma}_{(0)}^G \quad (k=1,\ldots,N-1)\end{aligned} \tag{35}$$

Alternatively, adopting Equation (29),

$$\begin{aligned}&\tfrac{1}{h^{(k+1)}}\mathbf{u}^{L(k+1)}-\left(\tfrac{1}{h^{(k)}}\left(\mathbf{I}+\mathbf{A}^{(k+1,k)}\right)+\tfrac{1}{h^{(k+1)}}\mathbf{I}\right)\mathbf{u}^{L(k+1)}+\tfrac{1}{h^{(k)}}\left(\mathbf{I}+\mathbf{A}^{(k+1,k)}\right)\mathbf{u}^{L(k-1)}\\ &=\mathbf{A}^{(k+1,k)}\boldsymbol{\gamma}_{(0)}^G \qquad (k=1,\ldots,N-1)\end{aligned} \tag{36}$$

where

$$\begin{aligned}&\mathbf{A}^{(k+1,k)}=-\overline{\mathbf{S}}_t^{(k+1)}\Delta\overline{\mathbf{Q}}_t^{(k+1,k)}=\overline{\mathbf{S}}_t^{(k+1)}\overline{\mathbf{Q}}_t^{(k)}-\mathbf{I};\\ &\Delta\overline{\mathbf{Q}}_t^{(k+1,k)}=\overline{\mathbf{Q}}_t^{(k+1)}-\overline{\mathbf{Q}}_t^{(k)}\end{aligned} \tag{37}$$

and $\overline{\mathbf{S}}_t^{(k)}=\left(\overline{\mathbf{Q}}_t^{(k)}\right)^{-1}$ is the transverse shear compliance matrix of the kth layer.

From Equation (35),

$$\Delta\boldsymbol{\gamma}^{L(k+1,k)}=\boldsymbol{\gamma}^{L(k+1)}-\boldsymbol{\gamma}^{L(k)}=\mathbf{A}^{L(k+1,k)}\left(\boldsymbol{\gamma}^{L(k)}+\boldsymbol{\gamma}_{(0)}^G\right)=\mathbf{A}^{L(k+1,k)}\boldsymbol{\gamma}^{(k)} \tag{38}$$

i.e., the jump in the slope between any two adjacent kth and $(k+1)$th layers is proportional to the slope $\boldsymbol{\gamma}^{(k)}$, which is assumed constant through the thickness of the kth layer in the FSDT global kinematics. The numerical value of the constant $\mathbf{A}^{(k+1,k)}$ depends only on the transverse shear stiffness properties of the two adjacent layers, as given in Equation (37). Thus, the $\mathbf{A}^{(k+1,k)}$, denoted here as the **zigzag effect index,** is responsible for the through-the-thickness variation in the slope in the local contribution of the in-plane displacements. In fact, from Equation (37),

$$\Delta\overline{\mathbf{Q}}_t^{(k+1,k)}=\mathbf{0}\Rightarrow\mathbf{A}^{(k+1,k)}=\mathbf{0} \tag{39}$$

i.e., the zigzag effect vanishes when two adjacent layers have the same transverse shear stiffnesses.

Obtaining a recursive expression for the local in-plane displacement contribution can be useful for practical applications. Elaborating further on Equation (35) (the details of the derivation are provided in Appendix A), the following recursive formula is obtained:

$$\boldsymbol{\gamma}^{L(k+1)}=\mathbf{a}^{L(k+1)}\boldsymbol{\gamma}^{L(1)}+\mathbf{a}^{(k+1)}\boldsymbol{\gamma}_{(0)}^G \tag{40}$$

where

$$\begin{aligned}\mathbf{a}^{(k+1)} &= \left(\mathbf{I}+\mathbf{A}^{(k+1,k)}\right)\mathbf{a}^{(k)}+\mathbf{A}^{(k+1,k)}\\ &= \mathbf{a}^{(k)}+\mathbf{A}^{(k+1,k)}\left(\mathbf{I}+\mathbf{a}^{(k)}\right) \qquad (k=1,\ldots,N-1)\end{aligned} \tag{41}$$

$$\begin{aligned}\mathbf{a}^{L(k+1)} &= \left(\mathbf{I}+\mathbf{A}^{(k+1,k)}\right)\left(\mathbf{I}+\mathbf{a}^{(k)}\right)\\ &= \overline{\mathbf{S}}_t^{(k+1)}\overline{\mathbf{Q}}_t^{(1)} \qquad (k=1,\ldots,N-1)\end{aligned} \tag{42}$$

and $\mathbf{a}^{(1)}=\mathbf{a}^{L(1)}=\mathbf{0}$. Combining Equations (41) and (42) yields

$$\mathbf{a}^{L(k+1)}=\mathbf{I}+\mathbf{a}^{(k+1)} \tag{43}$$

Furthermore, starting from the second form of Equation (41), the following relation that is valid for a generic kth layer can be obtained (the details of the derivation are provided in Appendix A):

$$\begin{aligned}\mathbf{a}^{(k+1)} &= \mathbf{A}^{(k+1,k)} + \overline{\mathbf{S}}_t^{(k+1)} \sum_{p=1}^{k-1} \overline{\mathbf{Q}}_t^{(p+1)} \mathbf{A}^{(p+1,p)} \\ &= \overline{\mathbf{S}}_t^{(k+1)} \sum_{p=1}^{k} \overline{\mathbf{Q}}_t^{(p+1)} \mathbf{A}^{(p+1,p)}\end{aligned} \tag{44}$$

Finally, adopting Equations (40) and (42), Equation (31) reads:

$$\mathbf{u}_{(k)}^L - \mathbf{u}_{(0)}^L = \left(\sum_{p=1}^{k} h^{(p)} \overline{\mathbf{S}}_t^{(p)} \right) \overline{\mathbf{Q}}_t^{(1)} \boldsymbol{\gamma}^{L(1)} + \left(\sum_{p=1}^{k} h^{(p)} \mathbf{a}^{(p)} \right) \boldsymbol{\gamma}_{(0)}^G \ \ (k = 1, \ldots, N) \tag{45}$$

It can be seen that the expression given by Equation (45) applies in general since it has been obtained directly from the interface continuity conditions for the in-plane displacements and transverse shear stresses. However, as anticipated, four unknown local contributions to the in-plane generalised displacements are free, and further constraint conditions are required to obtain a recursive formula.

In the following section, we will focus on three possible scenarios and present some considerations with existing methods.

2.7. Generalised Expressions for the Local In-Plane Displacement Zigzag Contribution

2.7.1. Scenario 1—ZZT$^{(0,1)}$

Following the original zigzag theory pioneered by Di Sciuva [21], who adopted a Heaviside step function to modulate the local in-plane displacement contribution, the same constraint conditions on the local transverse shear strains are enforced, i.e.,

$$\boldsymbol{\gamma}^{L(1)} = \boldsymbol{\theta}^{(1)} = \mathbf{0} \Rightarrow \mathbf{u}_B^{L(1)} = \mathbf{u}_T^{L(1)} = \mathbf{0} \Rightarrow \mathbf{u}_{(0)}^L = \mathbf{u}_{(1)}^L = \mathbf{0} \tag{46}$$

Using Equations (40), (42) and (44) yields

$$\boldsymbol{\gamma}^{L(k+1)} = \boldsymbol{\theta}^{L(k+1)} = \mathbf{a}^{(k+1)} \boldsymbol{\gamma}_{(0)}^G = \mathbf{a}_{ZZT^{(0,1)}}^{(k+1)} \boldsymbol{\gamma}_{(0)}^G \ \ (k = 1, \ldots, N-1) \tag{47}$$

where

$$\mathbf{a}_{ZZT^{(0,1)}}^{(k+1)} = \overline{\mathbf{S}}_t^{(k+1)} \sum_{p=1}^{k} \overline{\mathbf{Q}}_t^{(p+1)} \mathbf{A}^{(p+1,p)} \tag{48}$$

Substituting Equation (46) in Equation (45) yields

$$\mathbf{u}_{(k)}^L = \left(\sum_{p=1}^{k} h^{(p)} \mathbf{a}^{(p)} \right) \boldsymbol{\gamma}_{(0)}^G \ \ (k = 2, \ldots, N) \tag{49}$$

Taking a look at both Equations (47)–(49) and Ref. [22], it is understandable why the $\mathbf{a}^{(p)}$ terms have been called the *"continuity constants"*. In fact, they define in terms of $\boldsymbol{\gamma}_{(0)}^G$ the local contribution $\boldsymbol{\gamma}^{L(k)}$, i.e., Equation (47), and $\mathbf{u}_{(k)}^L$, i.e., Equation (49), which ensure the interface continuity of the transverse shear stresses.

Note that $\mathbf{a}^{(k+1)}$(see Equation (41)) gives the contribution of $\boldsymbol{\gamma}_{(0)}^G$ to the local slope in the kth layer, whereas $\mathbf{a}^{L(k+1)}$ (see Equation (42)) gives the contribution of $\boldsymbol{\gamma}^{L(1)}$ to the local slope in the kth layer as reported in Equation (40).

2.7.2. Scenario 2—ZZT$^{(0,N)}$

In the first-order ZZT$^{(0,N)}$, following Tessler et al. [29,33], we enforce the following conditions (it should be emphasised that the ZZT$^{(0,N)}$ derived in this paper uses the same constraints as the classical RZT (see Tessler et al. [33]), but differs from this one because ZZT$^{(0,N)}$ satisfies the continuity conditions on the full transverse shear stresses, contrary to the RZT of Tessler at al. [33], where the continuity conditions are imposed only on a part of the transverse shear stresses (see Section 2.8)):

$$\mathbf{u}_B^{L(1)} = \mathbf{u}_T^{L(N)} = \mathbf{0} \Rightarrow \mathbf{u}_{(0)}^{L} = \mathbf{u}_{(N)}^{L} = \mathbf{0} \tag{50}$$

It should be noted that the condition given by Equation (50) is a special case of that given by Equation (33).

Specifying Equation (45) for $k = N$ and taking into account Equation (50) yields

$$\mathbf{u}_{(N)}^{L} - \mathbf{u}_{(0)}^{L} = \overline{\mathbf{S}}_t \overline{\mathbf{Q}}_t^{(1)} \boldsymbol{\gamma}^{L(1)} + \mathbf{a}\boldsymbol{\gamma}_{(0)}^{G} = \mathbf{0} \tag{51}$$

where

$$\begin{aligned} \overline{\mathbf{S}}_t &= \sum_{p=1}^{N} h^{(p)} \overline{\mathbf{S}}_t^{(p)} = h\mathbf{G}^{-1} \\ \mathbf{a} &= \sum_{p=1}^{N} h^{(p)} \mathbf{a}^{(p)} \end{aligned} \tag{52}$$

and

$$\mathbf{G} = \left(\frac{1}{h} \overline{\mathbf{S}}_t \right)^{-1} = \left(\frac{1}{h} \sum_{p=1}^{N} h^{(p)} \overline{\mathbf{S}}_t^{(k)} \right)^{-1} \tag{53}$$

Observing the first term of Equation (52), it is easy to understand the physical meaning of matrix **G**: it is the matrix of the equivalent transverse shear stiffness coefficient of the laminated plate.

Solving Equation (51) for the $\overline{\mathbf{Q}}_t^{(1)} \boldsymbol{\gamma}^{L(1)}$ term and substituting it into Equation (45) yields

$$\mathbf{u}_{(k)}^{L} - \mathbf{u}_{(0)}^{L} = \left[-\frac{1}{h} \left(\sum_{p=1}^{k} h^{(p)} \overline{\mathbf{S}}_t^{(p)} \right) \mathbf{G}\mathbf{a} + \left(\sum_{p=1}^{k} h^{(p)} \mathbf{a}^{(p)} \right) \right] \boldsymbol{\gamma}_{(0)}^{G} \tag{54}$$

Now, let us express $\boldsymbol{\gamma}^{L(k)}$:

$$\boldsymbol{\gamma}^{L(k)} = \boldsymbol{\theta}^{L(k)} = \frac{\mathbf{u}_{(k)}^{L} - \mathbf{u}_{(k-1)}^{L}}{h^{(k)}} = \left(\mathbf{a}^{(k)} - \frac{1}{h} \overline{\mathbf{S}}_t^{(k)} \mathbf{G}\mathbf{a} \right) \boldsymbol{\gamma}_{(0)}^{G} = \mathbf{a}_{ZZT^{(0,N)}}^{(k)} \boldsymbol{\gamma}_{(0)}^{G} \tag{55}$$

where

$$\mathbf{a}_{ZZT^{(0,N)}}^{(k)} = \mathbf{a}^{(k)} - \frac{1}{h} \overline{\mathbf{S}}_t^{(k)} \mathbf{G}\mathbf{a} = \mathbf{a}_{ZZT^{(0,1)}}^{(k)} - \frac{1}{h} \overline{\mathbf{S}}_t^{(k)} \mathbf{G}\mathbf{a} \tag{56}$$

It can be shown (the details of the derivation are provided in Appendix B) that Equation (56) can be recast in the following recursive form, i.e., Equation (A17):

$$\mathbf{a}_{ZZT^{(0,N)}}^{(k)} = \overline{\mathbf{S}}_t^{(k)} \mathbf{G} - \mathbf{I} \tag{57}$$

2.7.3. Scenario 3—ZZT$^{(M0,M1)}$

Following an approach similar to that described in Kim and Cho's work [77], in this scenario, let us assume that $\mathbf{u}^{(0)}(\mathbf{x};t)$ and $\boldsymbol{\theta}(\mathbf{x};t)$ are the through-the-thickness averaged values of the axial displacement and rotation, respectively. In Kim and Cho's study [77], a set of warping functions of the transverse coordinate variable is introduced to enhance the multilayered plate's kinematics. As reported in Ref. [77], the constraint conditions are enforced in a least-square sense, to enhance the FSDT kinematics with respect to the

three-dimensional elasticity. Although the equations adopted are formally the same, the constraint conditions in scenario 3 have a different purpose, i.e., to fully characterise the in-plane local displacement contribution. According to this assumption, it is implied that the averaged values of the local contribution to the axial displacement and rotation, i.e., their moments of order 0 (M0) and 1 (M1), are forced to vanish. In formulas,

$$\left\langle \tilde{\mathbf{u}}^{L(k)}(\mathbf{X},t) \right\rangle = \mathbf{0} \tag{58}$$

$$\left\langle x_3 \tilde{\mathbf{u}}^{L(k)}(\mathbf{X},t) \right\rangle = \mathbf{0} \tag{59}$$

where the symbol $\langle(\cdot)\rangle$ stands for

$$\langle(\cdot)\rangle = \int_{z_{(0)}}^{z_{(N)}} (\cdot) dx_3 = \sum_{k=1}^{N} \int_{z_{(k-1)}}^{z_{(k)}} (\cdot) dx_3 = \sum_{k=1}^{N} \frac{h^{(k)}}{2} \int_{-1}^{+1} (\cdot) d\zeta \tag{60}$$

Substituting Equation (17) into Equations (58) and (59) yields to the following constraint conditions:

$$\sum_{k=1}^{N} \frac{h^{(k)}}{2} \left(\mathbf{u}^{L}_{(k)}(\mathbf{x};t) + \mathbf{u}^{L}_{(k-1)}(\mathbf{x};t) \right) = \mathbf{0} \tag{61}$$

$$\sum_{k=1}^{N} \frac{h^{(k)}}{2} \left(\left(z^{(k)}_{M} + \frac{h^{(k)}}{6} \right) \mathbf{u}^{L}_{(k)}(\mathbf{x};t) + \left(z^{(k)}_{M} - \frac{h^{(k)}}{6} \right) \mathbf{u}^{L}_{(k-1)}(\mathbf{x};t) \right) = \mathbf{0} \tag{62}$$

Let us express $\mathbf{u}^{L}_{(k)}$ and $\mathbf{u}^{L}_{(k-1)}$ using Equation (45)

$$\begin{aligned} \mathbf{u}^{L}_{(k)} = \; & \tfrac{1}{h^{(1)}} \left(\sum_{p=1}^{k} h^{(p)} \overline{\mathbf{S}}^{(p)}_{t} \right) \overline{\mathbf{Q}}^{(1)}_{t} \mathbf{u}^{L}_{(1)} + \left(\mathbf{I} - \tfrac{1}{h^{(1)}} \left(\sum_{p=1}^{k} h^{(p)} \overline{\mathbf{S}}^{(p)}_{t} \right) \overline{\mathbf{Q}}^{(1)}_{t} \right) \mathbf{u}^{L}_{(0)} \\ & + \left(\sum_{p=1}^{k} h^{(p)} \mathbf{a}^{(p)} \right) \boldsymbol{\gamma}^{G}_{(0)} \end{aligned} \tag{63}$$

$$\begin{aligned} \mathbf{u}^{L}_{(k-1)} = \; & \tfrac{1}{h^{(1)}} \left(\sum_{p=1}^{k-1} h^{(p)} \overline{\mathbf{S}}^{(p)}_{t} \right) \overline{\mathbf{Q}}^{(1)}_{t} \mathbf{u}^{L}_{(1)} + \left(\mathbf{I} - \tfrac{1}{h^{(1)}} \left(\sum_{p=1}^{k-1} h^{(p)} \overline{\mathbf{S}}^{(p)}_{t} \right) \overline{\mathbf{Q}}^{(1)}_{t} \right) \mathbf{u}^{L}_{(0)} \\ & + \left(\sum_{p=1}^{k-1} h^{(p)} \mathbf{a}^{(p)} \right) \boldsymbol{\gamma}^{G}_{(0)} \end{aligned} \tag{64}$$

Substituting Equations (63) and (64) into Equations (61) and (62), after some mathematical manipulations, yields the following system:

$$\begin{cases} \mathbf{C}^{0}_{1} \mathbf{u}^{L}_{(0)} + \mathbf{C}^{1}_{1} \mathbf{u}^{L}_{(1)} + \mathbf{C}^{G}_{1} \boldsymbol{\gamma}^{G}_{(0)} = \mathbf{0} \\ \mathbf{C}^{0}_{2} \mathbf{u}^{L}_{(0)} + \mathbf{C}^{1}_{2} \mathbf{u}^{L}_{(1)} + \mathbf{C}^{G}_{2} \boldsymbol{\gamma}^{G}_{(0)} = \mathbf{0} \end{cases} \tag{65}$$

where

$$\mathbf{C}^{0}_{1} = h\mathbf{I} - \mathbf{C}^{1}_{1};\; \mathbf{C}^{1}_{1} = \frac{1}{h^{(1)}} \overline{\mathbf{S}}^{*}_{t} \overline{\mathbf{Q}}^{(1)}_{t};\; \mathbf{C}^{G}_{1} = \mathbf{a}^{*} \tag{66}$$

$$\mathbf{C}^{0}_{2} = 2 \sum_{k=1}^{N} h^{(k)} \left(z^{(k)}_{M} - z_{B} \right) \mathbf{I} - \mathbf{C}^{1}_{2};\; \mathbf{C}^{1}_{2} = \frac{1}{h^{(1)}} \overline{\mathbf{S}}^{**}_{t} \overline{\mathbf{Q}}^{(1)}_{t};\; \mathbf{C}^{G}_{2} = \mathbf{a}^{**} \tag{67}$$

Moreover,

$$\overline{\mathbf{S}}^{*}_{t} = \sum_{k=1}^{N} h^{(k)} \left(\sum_{p=1}^{k-1} h^{(p)} \overline{\mathbf{S}}^{(p)}_{t} + \frac{h^{(k)}}{2} \overline{\mathbf{S}}^{(k)}_{t} \right) \tag{68}$$

$$\overline{\mathbf{S}}^{**}_{t} = \sum_{k=1}^{N} h^{(k)} \left[\left(z^{(k)}_{M} - z_{B} \right) 2 \left(\sum_{p=1}^{k-1} h^{(p)} \overline{\mathbf{S}}^{(p)}_{t} + \frac{h^{(k)}}{2} \overline{\mathbf{S}}^{(k)}_{t} \right) + \frac{h^{(k)2}}{6} \overline{\mathbf{S}}^{(k)}_{t} \right] \tag{69}$$

The expression for $\mathbf{a}^{*}$ and $\mathbf{a}^{**}$ can be easily obtained from Equations (68) and (69), by replacing $\overline{\mathbf{S}}_t^{(l)}$ with $\mathbf{a}^{(l)}$.

Note that $\mathbf{C}_\alpha^0, \mathbf{C}_\alpha^1, \mathbf{C}_\alpha^G$ $(\alpha = 1, 2)$ are 2×2 matrices whose entries are defined in terms of the layers' geometry (thicknesses) and mechanical properties (transverse shear stiffnesses). Therefore, once the lamination layout has been defined, they can be easily evaluated using MATLAB2023®/Python3.7.0™/Microsoft® Excel. Note that the elements of these matrices are independent of the individual layer. That is, they represent an average quantity: they have a similar role to the matrix **G** and the matrix of the sum of the coefficients **a** of $\mathrm{ZZT}^{(0,\mathrm{N})}$.

When the equation system, i.e., (65), is solved, the explicit expressions for $\mathbf{u}_{(0)}^L$ and $\mathbf{u}_{(1)}^L$ are obtained:

$$\mathbf{u}_{(0)}^L = \mathbf{C}_u^{(0)} \boldsymbol{\gamma}_{(0)}^G \tag{70}$$

$$\mathbf{u}_{(1)}^L = \mathbf{C}_u^{(1)} \boldsymbol{\gamma}_{(0)}^G \tag{71}$$

where

$$\mathbf{C}_u^{(1)} = \left(\mathbf{C}_2^1 - \mathbf{C}_2^0\left(\mathbf{C}_1^0\right)^{-1}\mathbf{C}_1^1\right)^{-1}\left(\mathbf{C}_2^0\left(\mathbf{C}_1^0\right)^{-1}\mathbf{C}_1^G - \mathbf{C}_2^G\right) \tag{72}$$

$$\mathbf{C}_u^{(0)} = -\left(\mathbf{C}_1^0\right)^{-1}\left(\mathbf{C}_1^G + \mathbf{C}_1^1\mathbf{C}_u^{(1)}\right) \tag{73}$$

Using relations (70) and (71) in Equation (63) yields

$$\begin{aligned}\mathbf{u}_{(k)}^L = \quad & \left(\mathbf{I} - \tfrac{1}{h^{(1)}}\left(\sum_{p=1}^{k} h^{(p)}\overline{\mathbf{S}}_t^{(p)}\right)\overline{\mathbf{Q}}_t^{(1)}\right)\mathbf{C}_u^{(0)} + \tfrac{1}{h^{(1)}}\left(\sum_{p=1}^{k} h^{(p)}\overline{\mathbf{S}}_t^{(p)}\right)\overline{\mathbf{Q}}_t^{(1)}\mathbf{C}_u^{(1)} \\ & + \left(\sum_{p=1}^{k} h^{(p)}\mathbf{a}^{(p)}\right)\boldsymbol{\gamma}_{(0)}^G\end{aligned} \tag{74}$$

In analogy to what has been done in $\mathrm{ZZT}^{(0,1)}$ and $\mathrm{ZZT}^{(0,\mathrm{N})}$, the next step is to express $\boldsymbol{\gamma}^{L(k)}$ as a function of $\boldsymbol{\gamma}_{(0)}^G$.

Starting from Equation (45),

$$\boldsymbol{\gamma}^{L(k)} = \frac{\mathbf{u}_{(k)}^L - \mathbf{u}_{(k-1)}^L}{h^{(k)}} = \frac{1}{h^{(1)}}\overline{\mathbf{S}}_t^{(1)}\overline{\mathbf{Q}}_t^{(1)}\left(\mathbf{u}_{(1)}^L - \mathbf{u}_{(0)}^L\right) + \mathbf{a}^{(k)}\boldsymbol{\gamma}_{(0)}^G \tag{75}$$

and substituting Equations (70) and (71) into Equation (75) yields

$$\boldsymbol{\gamma}^{L(k)} = \mathbf{a}_{ZZT^{(M0,M1)}}^{(k)}\boldsymbol{\gamma}_{(0)}^G \tag{76}$$

with

$$\begin{aligned}\mathbf{a}_{ZZT^{(M0,M1)}}^{(k)} &= \tfrac{1}{h^{(1)}}\overline{\mathbf{S}}_t^{(k)}\overline{\mathbf{Q}}_t^{(1)}\left(\mathbf{C}_u^{(1)} - \mathbf{C}_u^{(0)}\right) + \mathbf{a}^{(k)} = \mathbf{a}^{(k)} - \tfrac{1}{h}\overline{\mathbf{S}}_t^{(k)}\mathbf{G}^a \\ &= \mathbf{a}_{ZZT^{(0,1)}}^{(k)} - \tfrac{1}{h}\overline{\mathbf{S}}_t^{(k)}\mathbf{G}^a\end{aligned} \tag{77}$$

$$\mathbf{G}^a = -\frac{h}{h^{(1)}}\overline{\mathbf{Q}}_t^{(1)}\left(\mathbf{C}_u^{(1)} - \mathbf{C}_u^{(0)}\right) \tag{78}$$

In closing this section, taking advantage of the previous results, we can deduce the following general expression for the local contribution in all three previous scenarios:

$$\boldsymbol{\gamma}^{L(k)} = \boldsymbol{\theta}^{L(k)} = \boldsymbol{\beta}^{(k)}\boldsymbol{\gamma}_{(0)}^G \tag{79}$$

Using Equation (79) in Equation (31) and remembering Equation (70), the expression for the in-plane local displacement contributions evaluated at the kth interface is as follows:

$$\mathbf{u}^L_{(k)} = \left(\sum_{p=1}^{k} h^{(p)} \boldsymbol{\beta}^{(p)} \right) \boldsymbol{\gamma}^G_{(0)} + \mathbf{C}^{(0)}_u \boldsymbol{\gamma}^G_{(0)} = \boldsymbol{\varphi}_{(k)} \boldsymbol{\gamma}^G_{(0)} \tag{80}$$

where

$$\boldsymbol{\varphi}_{(k)} = \sum_{p=1}^{k} h^{(p)} \boldsymbol{\beta}^{(p)} + \mathbf{C}^{(0)}_u \tag{81}$$

In Equation (81), $\mathbf{C}^{(0)}_u = \mathbf{0}$ in both ZZT$^{(0,1)}$ and ZZT$^{(0,N)}$.

Table 1 summarises the expressions of $\boldsymbol{\beta}^{(k)}$ for the three proposed scenarios.

Table 1. Summary of the expressions for $\boldsymbol{\beta}^{(k)}$ using the three scenarios for ZZT.

Scenario	Continuity Constant $\boldsymbol{\beta}^{(k)}$	Reference Equation
ZZT$^{(0,1)}$	$\boldsymbol{\beta}^{(k)} = \mathbf{a}^{(k)}_{ZZT^{(0,1)}} = \mathbf{a}^{(k)}$	Equation (47)
ZZT$^{(0,N)}$	$\boldsymbol{\beta}^{(k)} = \mathbf{a}^{(k)}_{ZZT^{(0,N)}} = \mathbf{a}^{(k)} - \frac{1}{h}\overline{\mathbf{S}}^{(k)}_t \mathbf{G}\mathbf{a}$	Equation (55)
ZZT$^{(M0,M1)}$	$\boldsymbol{\beta}^{(k)} = \mathbf{a}^{(k)}_{ZZT^{(M0,M1)}} = \mathbf{a}^{(k)}_{ZZT^{(0,1)}} - \frac{1}{h}\overline{\mathbf{S}}^{(k)}_t \mathbf{G}^a$	Equation (76)

It is interesting to note that $\mathbf{a}^{(k)}$ always appears in the expressions, as it derives from the continuity of the transverse shear stresses at the interfaces, which is a constraint common to all methods. Clearly, other choices available in the current literature are also possible, e.g., Averill's method.

2.8. Refined Zigzag Theories

In the previous sections, it has been demonstrated (Equation (45)) that while satisfying the interlaminar conditions at each layer interface, i.e., displacement and transverse shear stress continuities, the local layer-wise contribution to the in-plane displacement can be expressed in the following general statement, here reported for clarity:

$$\mathbf{u}^L_{(k)} - \mathbf{u}^L_{(0)} = \left(\sum_{p=1}^{k} h^{(p)} \overline{\mathbf{S}}^{(p)}_t \right) \overline{\mathbf{Q}}^{(1)}_t \boldsymbol{\gamma}^{L(1)} + \left(\sum_{p=1}^{k} h^{(p)} \mathbf{a}^{(p)} \right) \boldsymbol{\gamma}^G_{(0)} \quad (k = 1, \ldots, N) \tag{82}$$

As argued extensively in the above section, four free unknowns related to the local in-plane displacements are still present in Equation (82); thus, appropriate choices are required to characterise its through-the-thickness distribution fully. Three scenarios have been presented, and each of them is able to determine the remaining unknowns uniquely. At least for them and for linear-based kinematics, the following general result is obtained:

$$\boldsymbol{\gamma}^{L(k+1)} = \mathbf{a}^{L(k+1)} \boldsymbol{\gamma}^{L(1)} + \mathbf{a}^{(k+1)} \boldsymbol{\gamma}^G_{(0)} \rightarrow \boldsymbol{\gamma}^{L(k)} = \boldsymbol{\beta}^{(k)} \boldsymbol{\gamma}^G_{(0)} \tag{83}$$

with $\boldsymbol{\beta}^{(k)}$ given in Table 1 and $\boldsymbol{\gamma}^G_{(0)}$ expressed by Equation (25).

As recalled in the Introduction, such zigzag functions suffer from some drawbacks (shortcomings) that motivated Tessler et al. [29,33] to partially release the constraints on the continuity of transverse shear stresses. In fact, looking at the expression of the local displacements' contribution, i.e., Equation (82), when clamped boundary conditions are considered, the transverse shear strain $\boldsymbol{\gamma}^G_{(0)}$ must vanish. Consequently, the transverse shear stresses and force resultants vanish, leading to the same inconsistency of Reddy's third-order shear deformation theory.

In order to solve this issue, the transverse shear strain that appears in Equation (83) is substituted by a new couple of additional independent kinematic variables, denoted with $\boldsymbol{\psi}(\mathbf{x}; t)$, that relax the transverse shear stress continuity at the layer interfaces. Thus, the

interlaminar stress continuity is limited to the local contribution to the transverse shear stresses. The resulting zigzag theory has been called refined zigzag theory (RZT), and it involves seven kinematic unknowns for the plate model.

Thus, the local transverse shear strain, i.e., Equation (83), reads

$$\boldsymbol{\gamma}^{L(k)}(\mathbf{x}) = \boldsymbol{\beta}^{(k)}\boldsymbol{\psi}(\mathbf{x}) \tag{84}$$

where the $\boldsymbol{\beta}^{(k)}$ values are the same as those listed in Table 1, here reported for completeness.

Thus, the local in-plane contributions, Equation (80), holds with $\boldsymbol{\gamma}^{G}_{(0)}$ replaced by $\boldsymbol{\psi}$, representing the zigzag rotations,

$$\mathbf{u}^{L}_{(k)} = \left(\sum_{p=1}^{k} h^{(p)}\boldsymbol{\beta}^{(p)}\right)\boldsymbol{\psi} + \mathbf{u}^{L}_{(0)} \tag{85}$$

Before proceeding further, for convenience, Equations (80) and (85) can be further generalised to take into consideration both RZT and ZZT first-order kinematics. For each kth layer interface, we write

$$\begin{aligned}
\mathbf{u}^{L}_{(k)} = & \left(\sum_{p=1}^{k} h^{(p)}\boldsymbol{\beta}^{(p)}\right)\left(\kappa_{ZZT}\boldsymbol{\gamma}^{G}_{(0)} + \kappa_{RZT}\boldsymbol{\psi}\right) + \kappa_{M0M1}\mathbf{u}^{L}_{(0)} \\
& = \boldsymbol{\varphi}_{(k)}\left(\kappa_{ZZT}\boldsymbol{\gamma}^{G}_{(0)} + \kappa_{RZT}\boldsymbol{\psi}\right) + \kappa_{M0M1}\mathbf{u}^{L}_{(0)} \\
& = \boldsymbol{\varphi}_{(k)}\left(\kappa_{ZZT}\boldsymbol{\gamma}^{G}_{(0)} + \kappa_{RZT}\boldsymbol{\psi}\right) + \kappa_{M0M1}\mathbf{C}^{(0)}_{u}\left(\kappa_{ZZT}\boldsymbol{\gamma}^{G}_{(0)} + \kappa_{RZT}\boldsymbol{\psi}\right) \\
& = \left(\boldsymbol{\varphi}_{(k)} + \kappa_{M0M1}\mathbf{C}^{(0)}_{u}\right)\left(\kappa_{ZZT}\boldsymbol{\gamma}^{G}_{(0)} + \kappa_{RZT}\boldsymbol{\psi}\right)
\end{aligned} \tag{86}$$

with κ_{ZZT} and κ_{RZT} being trace operators, respectively, for ZZT and RZT kinematics. More specifically, by setting $\kappa_{ZZT} = 1$ and $\kappa_{RZT} = 0$, Equation (86) gives the local interface displacement contributions of the first-order ZZT (see Table 1), whereas by setting $\kappa_{ZZT} = 0$ and $\kappa_{RZT} = 1$, Equation (86) gives the local contribution of the first-order RZT (see Table 2). Clearly, the cases $\kappa_{ZZT} = \kappa_{RZT} = 1$ and $\kappa_{ZZT} = \kappa_{RZT} = 0$ cannot coexist at the same time. The trace operator $\kappa_{M0M1} = 1$ for ZZT$^{(M0,M1)}$ or for RZT$^{(M0,M1)}$; otherwise, it is zero. Obviously, the result obtained for $\mathbf{u}^{L}_{(0)}$ for ZZT$^{(M0,M1)}$ (see Equation (70)) is also valid for RZT$^{(M0,M1)}$ after $\boldsymbol{\gamma}^{G}_{(0)}$ is replaced with $\boldsymbol{\psi}$.

Table 2. Summary of the expressions of $\boldsymbol{\beta}^{(k)}$ using the three scenarios for RZT.

Scenario	Continuity Constant $\boldsymbol{\beta}^{(k)}$	Reference Equation
RZT$^{(0,1)}$	$\boldsymbol{\beta}^{(k)} = \mathbf{a}^{(k)}_{RZT^{(0,1)}} = \mathbf{a}^{(k)}$	Equation (47)
RZT$^{(0,N)}$	$\boldsymbol{\beta}^{(k)} = \mathbf{a}^{(k)}_{RZT^{(0,N)}} = \mathbf{a}^{(k)} - \frac{1}{h}\bar{\mathbf{S}}^{(k)}_{t}\mathbf{G}\mathbf{a}$	Equation (55)
RZT$^{(M0,M1)}$	$\boldsymbol{\beta}^{(k)} = \mathbf{a}^{(k)}_{RZT^{(M0,M1)}} = \mathbf{a}^{(k)} - \frac{1}{h}\bar{\mathbf{S}}^{(k)}_{t}\mathbf{G}^{a}$	Equation (76)

Within each kth layer, using Equations (17) and (86) yields

$$\begin{aligned}
\tilde{\mathbf{u}}^{L(k)} & = \mathbf{u}^{L(k)}_{B}L_{B}(\zeta) + \mathbf{u}^{L(k)}_{T}L_{T}(\zeta) = \mathbf{u}^{L}_{(k-1)}L_{B}(\zeta) + \mathbf{u}^{L}_{(k)}L_{T}(\zeta) \\
& = \frac{1}{2}\Big[\left(2\boldsymbol{\varphi}_{(k-1)} + h^{(k)}\boldsymbol{\beta}^{(k)}\right)\left(\kappa_{ZZT}\boldsymbol{\gamma}^{G}_{(0)} + \kappa_{RZT}\boldsymbol{\psi}\right) + 2\kappa_{M0M1}\mathbf{u}^{L}_{(0)} \\
& + \zeta h^{(k)}\boldsymbol{\beta}^{(k)}\left(\kappa_{ZZT}\boldsymbol{\gamma}^{G}_{(0)} + \kappa_{RZT}\boldsymbol{\psi}\right)\Big]
\end{aligned} \tag{87}$$

Finally,

$$\begin{aligned}
\tilde{\mathbf{u}}^{L(k)} - \kappa_{M0M1}\mathbf{u}^{L}_{(0)} & = \left(\boldsymbol{\varphi}_{(k-1)} + \frac{1}{2}\left(1 + \zeta^{(k)}\right)h^{(k)}\boldsymbol{\beta}^{(k)}\right)\left(\kappa_{ZZT}\boldsymbol{\gamma}^{G}_{(0)} + \kappa_{RZT}\boldsymbol{\psi}\right) \\
& = \boldsymbol{\varphi}^{(k)}(\zeta)\left(\kappa_{ZZT}\boldsymbol{\gamma}^{G}_{(0)} + \kappa_{RZT}\boldsymbol{\psi}\right)
\end{aligned} \tag{88}$$

Introducing Equation (2) into Equation (88) yields

$$\begin{aligned}\boldsymbol{\varphi}^{(k)}(x_3) &= \boldsymbol{\varphi}_{(k-1)} + \tfrac{1}{2}h^{(k)}\boldsymbol{\beta}^{(k)} + \tfrac{1}{h^{(k)}}\left(x_3 - z_M^{(k)}\right)h^{(k)}\boldsymbol{\beta}^{(k)} \\ &= \boldsymbol{\varphi}_{(k-1)} + \left(x_3 - z_{(k)}\right)\boldsymbol{\beta}^{(k)}\end{aligned} \tag{89}$$

And using Equation (5) in Equation (89), we obtain

$$\boldsymbol{\varphi}^{(k)}(x_3) = \boldsymbol{\varphi}_{(0)} + \sum_{p=1}^{k-1} h^{(p)}\left(\boldsymbol{\beta}^{(p)} - \boldsymbol{\beta}^{(k)}\right) + (x_3 - z_B)\boldsymbol{\beta}^{(k)} \tag{90}$$

which, for RZT$^{(0,N)}$ where $\boldsymbol{\varphi}_{(0)} = \mathbf{0}$, is the same as that reported in Ref. [34].

2.9. Generalised Plate's Governing Equations and Consistent Boundary Conditions

In this section, the governing equations of the first-order zigzag theories for multilayered plates are derived through the dynamic version of the principle of virtual displacements (PVD), also known as d'Alembert's principle. In order to keep the formulation as general as possible, the trace operators previously introduced and defined, i.e., κ_{ZZT}, κ_{RZT} and κ_{M0M1}, are included in the following derivation.

Introducing the variational operator δ, the PVD can be stated as follows:

$$\delta W_{int} = \delta W_{ext} + \delta W_{in} \tag{91}$$

where

$$\delta W_{int} = \int_{\Omega} \left\langle \tilde{\boldsymbol{\sigma}}_p^{(k)T} \delta\tilde{\mathbf{E}}_p^{(k)} + \tilde{\boldsymbol{\sigma}}_t^{(k)T} \delta\tilde{\boldsymbol{\gamma}}_t^{(k)} \right\rangle d\Omega \tag{92}$$

is the virtual variation in the strain energy;

$$\delta W_{in} = -\int_{\Omega} \left\langle \rho^{(k)} \left(\ddot{\tilde{\mathbf{u}}}^T \delta\tilde{\mathbf{u}} + \ddot{u}_3^{(0)} \delta u_3^{(0)} \right) \right\rangle d\Omega \tag{93}$$

is the virtual variation in the work done by the inertia forces, and $\rho^{(k)}$ is the material mass density of the kth layer. The overdot indicates differentiation with respect to the time.

Assuming that the plate is loaded only by transverse load pressures $\overline{p}_B(\mathbf{x};t)$ and $\overline{p}_T(\mathbf{x};t)$ acting, respectively, on the bottom and top external plate surfaces, the virtual variation in the work done by external loads reads

$$\delta W_{ext} = \int_{\Omega} (\overline{p}_B + \overline{p}_T)\delta u_3^{(0)} d\Omega = \int_{\Omega} \overline{p}_3 \delta u_3^{(0)} d\Omega \tag{94}$$

By substituting the expressions for displacements, i.e., Equations (15) and (87); strains, i.e., Equation (21); and stresses, i.e., Equation (22), into the governing functional, i.e., Equation (91), and integrating by parts (for the sake of clarity, the mathematical passages are provided in Appendix C), collecting and setting to zero the contributions multiplying the same virtual variation in the surface and boundary integrals yields the following **governing equations:**

$$\delta u_\alpha^{(0)}) \quad \mathbf{N}_\alpha^T \overleftarrow{\nabla} = m^{(0)}\ddot{u}_\alpha^{(0)} + m^{(1)}\ddot{\theta}_\alpha + \left(m_{\alpha\beta}^{\phi(0)} + m_{\alpha\beta}^{C(0)}\right)\left(\kappa_{ZZT}\left(\ddot{\theta}_\beta + \ddot{u}_{3,\beta}^{(0)}\right) + \kappa_{RZT}\ddot{\psi}_\beta\right) \tag{95}$$

$$\begin{aligned}\delta u_3^{(0)}) \quad & \left(\mathbf{Q}^T - \kappa_{ZZT}\mathbf{Q}^{\phi T}\right)\overleftarrow{\nabla} - \kappa_{ZZT}\left(\left(\mathbf{M}_\alpha^{\phi T} + \mathbf{M}_\alpha^{CT}\right)\overleftarrow{\nabla}\right)_{,\alpha} \\ & = -\overline{p}_3 + m^{(0)}\ddot{u}_3^{(0)} - \kappa_{ZZT}\left[\left(m_{\alpha\beta}^{\phi(0)} + m_{\alpha\beta}^{C(0)}\right)\ddot{u}_{3,\beta}^{(0)} + \left(m_{\alpha\beta}^{\phi(1)} + m_{\alpha\beta}^{C(1)}\right)\ddot{\theta}_{\beta,\alpha}\right. \\ & \left. + \left(m_{\beta\alpha}^{\phi\phi(0)} + m_{\beta\alpha}^{C(0)} + m_{\beta\alpha}^{\phi C(0)} + m_{\beta\alpha}^{CC(0)}\right)\left(\ddot{\theta}_\beta + \ddot{u}_{3,\beta}^{(0)}\right)_{,\alpha}\right]\end{aligned} \tag{96}$$

$$\begin{aligned}\delta\theta_\alpha) \quad & \left(\mathbf{M}_\alpha^T + \kappa_{ZZT}\left(\mathbf{M}_\alpha^{\phi T} + \mathbf{M}_\alpha^{CT}\right)\right)\overleftarrow{\nabla} - Q_\alpha - \kappa_{ZZT}Q_\alpha^\phi \\ & = m^{(1)}\ddot{u}_\alpha^{(0)} + m^{(2)}\ddot{\theta}_\alpha + \left(m_{\alpha\beta}^{\phi(1)} + m_{\alpha\beta}^{C(1)}\right)\left(\kappa_{ZZT}\left(\ddot{\theta}_\beta + \ddot{u}_{3,\beta}^{(0)}\right) + \kappa_{RZT}\ddot{\psi}_\beta\right)\end{aligned} \tag{97}$$

$$\begin{aligned}\delta\psi_\alpha) \quad \kappa_{RZT}\left[\left(\mathbf{M}_\alpha^{\phi T} + \mathbf{M}_\alpha^{CT}\right)\overleftarrow{\nabla} - Q_\alpha^\phi\right] & = \kappa_{RZT}\left[\left(m_{\alpha\beta}^{\phi(0)} + m_{\alpha\beta}^{C(0)}\right)\ddot{u}_\alpha^{(0)} + \left(m_{\alpha\beta}^{\phi(1)} + m_{\alpha\beta}^{C(1)}\right)\ddot{\theta}_\alpha\right. \\ & \left. + \left(m_{\beta\alpha}^{\phi\phi(0)} + m_{\beta\alpha}^{C(0)} + m_{\beta\alpha}^{\phi C(0)} + m_{\beta\alpha}^{CC(0)}\right)\ddot{\psi}_\beta\right]\end{aligned} \tag{98}$$

and the consistent **boundary conditions**

$$\begin{array}{ccc} \text{Prescribed on } \Gamma_u & & \text{Prescribed on } \Gamma_\sigma \\ u_n^{(0)} & \vee & N_n \\ u_s^{(0)} & \vee & N_s \\ u_3^{(0)} & \vee & -\left(M_s^\phi + M_s^C\right)_{,s} + \mathbf{Q}^T\nabla_n + \kappa_{ZZT}\mathbf{Q}^{\phi T}\nabla_n + \\ & & -\kappa_{ZZT}n_\alpha\left(\left(\mathbf{M}_\alpha^{\phi T} + \mathbf{M}_\alpha^{CT}\right)\overleftarrow{\nabla}\right) + \\ & & -\kappa_{ZZT}n_\alpha\left[\left(m_{\alpha\beta}^{\phi(0)} + m_{\alpha\beta}^{C(0)}\right)\ddot{u}_3^{(0)} + \left(m_{\alpha\beta}^{\phi(1)} + m_{\alpha\beta}^{C(1)}\right)\ddot{\theta}_\beta + \right. \\ & & \left. + \left(m_{\beta\alpha}^{\phi\phi(0)} + m_{\beta\alpha}^{C(0)} + m_{\beta\alpha}^{\phi C(0)} + m_{\beta\alpha}^{CC(0)}\right)\left(\ddot{\theta}_\beta + \ddot{u}_{3,\beta}^{(0)}\right)\right] \\ \kappa_{ZZT}u_{3,n}^{(0)} & \vee & \kappa_{ZZT}\left(M_n^\phi + M_n^C\right) \\ \theta_n & \vee & M_n + \kappa_{ZZT}\left(M_n^\phi + M_n^C\right) \\ \theta_s & \vee & M_s + \kappa_{ZZT}\left(M_s^\phi + M_s^C\right) \\ \kappa_{RZT}\psi_n & \vee & \kappa_{RZT}\left(M_n^\phi + M_n^C\right) \\ \kappa_{RZT}\psi_s & \vee & \kappa_{RZT}\left(M_s^\phi + M_s^C\right) \end{array} \tag{99}$$

where the full expressions of the force/moment stress and inertia resultants are reported in Appendix C.

3. Numerical Analysis and Discussion

This section reports the numerical tests performed on the elastodynamic characteristics (static response and natural frequencies) of multilayered laminated plates. Since the accuracy and reliability of both ZZT and RZT models have been widely addressed in the open literature, no particular emphasis is given to their predictivity capabilities. On the other hand, the differences and equivalencies in the various scenarios for characterising the zigzag contribution and in predicting the structural behaviour are well addressed.

To pursue this aim, a first comparison is dedicated to evaluating the different scenarios describing the zigzag contributions. Two lamination schemes are considered: a symmetric sandwich (S) and a monolithic cross-ply laminate (L). Their properties and lamination stacking sequences are reported in Tables 3 and 4, respectively.

Table 3. Mechanical properties of the unidirectional layers (Young's and shear moduli are given in MPa, the material mass density in kg/m^3).

Material Name	E_1	E_2	E_3	ν_{12}	ν_{13}	ν_{23}	G_{12}	G_{13}	G_{23}	ρ
A	25	1	1	0.25	0.25	0.25	0.5	0.5	0.2	0.001
B	110,000	7857	7857	0.33	0.33	0.49	3292	3292	1292	-
C	40.3	40.3	40.3	0.3	0.3	0.3	12	12	12	-

Table 4. Laminate stacking sequences and nomenclatures (from bottom to top surface).

Laminate ID	Materials	$h^{(k)}/h$	Lamina Orientation [deg]
L	[A/A/A]	[0.25/0.5/0.25]	[0/90/0]
S	[B/B/C/B/B]	[0.05/0.05/0.8/0.05/0.05]	[0/90/0/90/0]

In the bending and free-vibration analysis, a square plate ($a/b = 1$) (the dimensions of which along x_1 and x_2 are defined with the symbols a and b, respectively), simply supported on all edges, with length-to-thickness ratio $a/h = 10$ is considered. For the static case, a bi-sinusoidal transverse intensity pressure $\overline{p}_3$ is applied and equally divided between the bottom and top external surfaces to reduce the effect of the transverse normal deformability in the three-dimensional exact solution. Due to the lamination scheme, load and boundary conditions, the exact Navier-type solution is obtained using the following trigonometric expression for the kinematic variables:

$$\begin{aligned}
&\left\{\begin{array}{c} u \\ \theta_1 \\ \psi_1 \end{array}\right\}(\mathbf{x};t) = \sum_{m=1}^{M}\sum_{n=1}^{N}\left\{\begin{array}{c} U \\ \Theta_1 \\ \Psi_1 \end{array}\right\}^{(mn)} \cos(\lambda_m x_1)\sin(\lambda_n x_2)\sin(\omega_{mn}t) \\
&\left\{\begin{array}{c} v \\ \theta_2 \\ \psi_2 \end{array}\right\}(\mathbf{x};t) = \sum_{m=1}^{M}\sum_{n=1}^{N}\left\{\begin{array}{c} V \\ \Theta_2 \\ \Psi_2 \end{array}\right\}^{(mn)} \sin(\lambda_m x_1)\cos(\lambda_n x_2)\sin(\omega_{mn}t) \\
&w(\mathbf{x};t) = \sum_{m=1}^{M}\sum_{n=1}^{N} W^{(mn)}\sin(\lambda_m x_1)\sin(\lambda_n x_2)\sin(\omega_{mn}t)
\end{aligned} \tag{100}$$

where $\lambda_m = \frac{m\pi}{a}$ and $\lambda_n = \frac{n\pi}{b}$ (m and n are the half-wave numbers in x_1 and x_2 directions, respectively). Moreover, ω_{mn} is the mnth undamped circular frequency, and $\left(U^{(mn)}, V^{(mn)}, W, \Theta_1^{(mn)}, \Theta_2^{(mn)}, \Psi_1^{(mn)}, \Psi_2^{(mn)}\right)$ are the unknown kinematic variables. Note that for bending analysis, $m = n = 1$.

The results considered in this numerical study concerning displacements and stresses are normalised as follows:

$$\begin{aligned}
&\overline{u}_\alpha^{(k)} = \frac{10^3 E_2^{(1)}}{\overline{p}_3 (a/h)^3}\widetilde{u}_\alpha^{(k)}; \overline{u}_3^{(k)} = \frac{10^2 E_2^{(1)}}{\overline{p}_3 (a/h)^4}\widetilde{u}_3^{(k)}; \\
&\left(\overline{\sigma}_{\alpha\alpha}^{(k)}, \overline{\tau}_{12}^{(k)}\right) = \frac{E_2^{(1)}}{\overline{p}_3 (a/h)^2}\left(\sigma_{\alpha\alpha}^{(k)}, \tau_{12}^{(k)}\right); \overline{\tau}_{\alpha 3}^{(k)} = \frac{10 E_2^{(1)}}{\overline{p}_3 (a/h)^2}\tau_{\alpha 3}^{(k)}; \\
&\overline{\omega}_{mn} = \omega_{mn} a\sqrt{\frac{E_2^{(1)}}{\rho^{(1)}}}
\end{aligned} \tag{101}$$

3.1. Zigzag Functions $\boldsymbol{\varphi}^{(k)}(x_3)$

Here, a brief comparison among the investigated scenarios for describing the zigzag contribution is proposed. More specifically, in this subsection, the through-the-thickness distributions of the $\boldsymbol{\varphi}^{(k)}(x_3)$ function are addressed. The considered laminates are those reported in Table 4. As detailed in the previous sections, it is worth noting that the expression for $\boldsymbol{\varphi}_{(k)}$ (see Equations (80) and (85)), which represents the values at the interfaces computed using the $\boldsymbol{\beta}^{(k)}$ expression given in Tables 1 and 2 for the three scenarios, is formally the same for both ZZT and RZT. As a consequence, the expression of $\boldsymbol{\varphi}^{(k)}(x_3)$ (as given by Equations (89) and (90)) is valid for both ZZT and RZT, since it does not depend on the assumed first-order zigzag kinematics. However, as detailed earlier, the three scenarios, i.e., scenario 1, ZZT/RZT$^{(0,1)}$; scenario 2, ZZT/RZT$^{(0,N)}$; and scenario 3, ZZT/RZT$^{(M0,M1)}$, differ in how the constraint conditions are imposed to achieve the expression of the local zigzag displacements. Note that the coupling zigzag functions vanish for the considered lamination schemes, i.e., L and S, the coupling zigzag functions vanish, i.e., $\varphi_{12}^{(k)} = \varphi_{21}^{(k)} = 0$; thus, they are not reported in the following examples.

Figures 3 and 4 show the distributions of the zigzag functions, i.e., the zigzag functions $\boldsymbol{\varphi}^{(k)}(x_3)$, through the laminate thickness for laminate L and sandwich S, respectively.

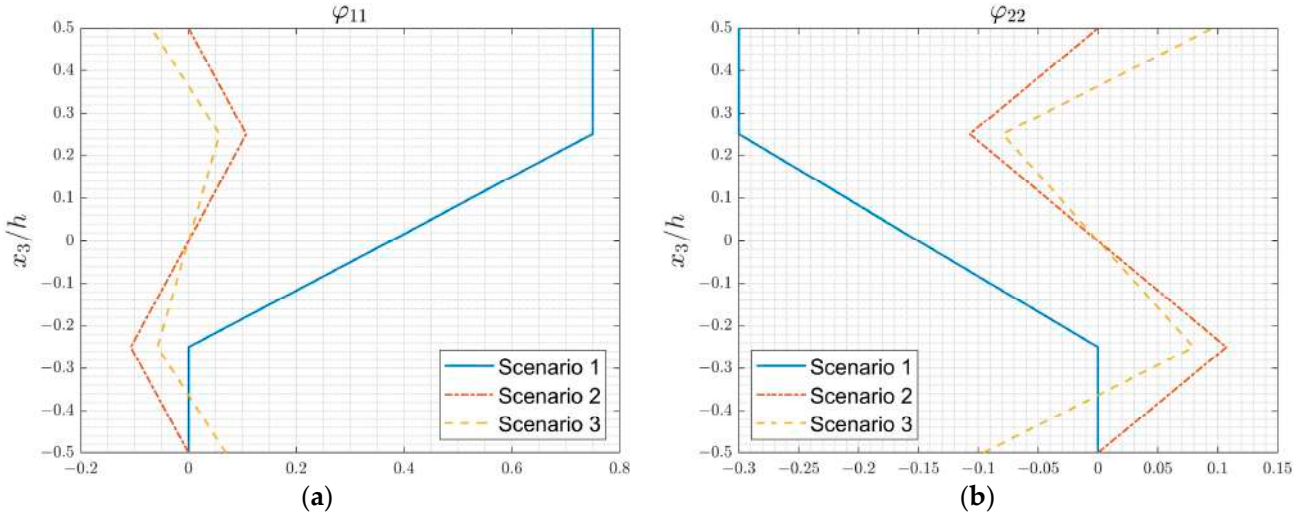

Figure 3. Through-the-thickness distributions of the zigzag contribution, i.e., (**a**) $\varphi_{11}^{(k)}(x_3)$ and (**b**) $\varphi_{22}^{(k)}(x_3)$, for laminate L.

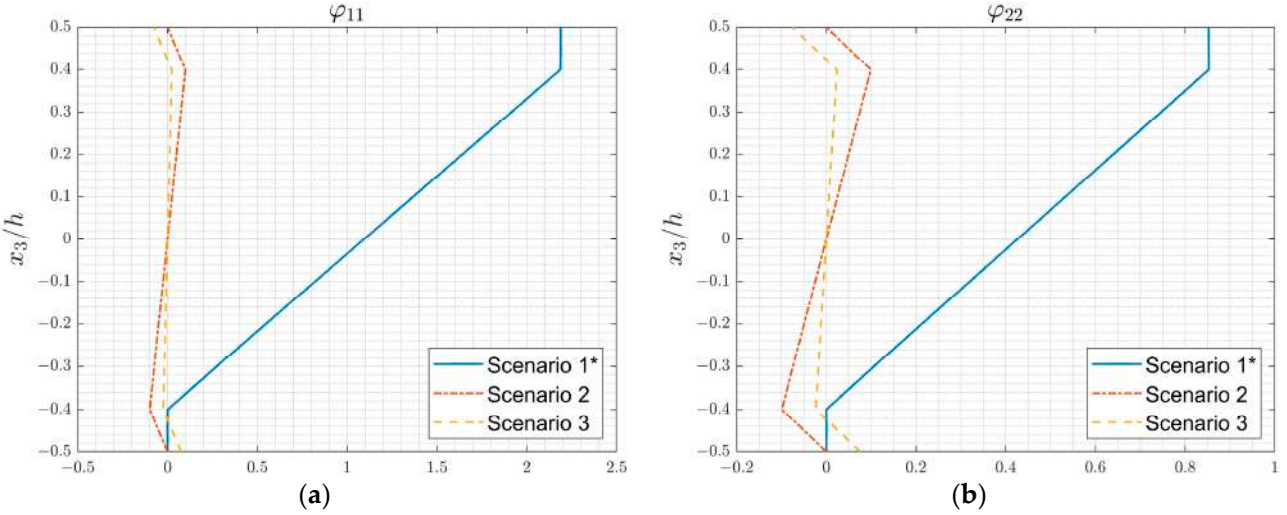

Figure 4. Through-the-thickness distributions of the zigzag contribution, i.e., (**a**) $\varphi_{11}^{(k)}(x_3)$ and (**b**) $\varphi_{22}^{(k)}(x_3)$, for sandwich S (* for scenario 1, the values are divided by 100).

It is interesting to note that scenario 1, characterising the zigzag effect, yields a greater contribution with respect to the other scenarios. This is due to the constraint condition of scenario 1, which is applied on the first layer. On the other hand, scenarios 2 and 3 enforce conditions in an average manner by considering integrals across the whole laminate; thus, the effect in the zigzag distributions is different but similar between them.

As expected, for the sandwich configuration, the core layer exhibits higher transverse deformability (which can be easily seen in scenario 1, where the slope is remarkably high), whereas for cross-ply laminate L, the transverse deformability is quite similar, and fewer differences are noticeable among the proposed scenarios.

However, it should be remembered for both laminate configurations and, in general, that the reported zigzag effect must be modulated by the appropriate rotations, namely $\gamma^{G}_{(0)}$ or ψ when ZZT or RZT is considered, respectively. Thus, it is expected that the model kinematics governs the overall plate behaviour and not the scenario characterising the zigzag distribution.

3.2. Bending Analysis

This example presents a numerical comparison of the bending behaviour computed using ZZT and RZT, adopting the different scenarios.

More specifically, Tables 5 and 6 report some numerical results concerning normalised displacements and stresses evaluated using ZZT and RZT at two interfaces, i.e., the bottom plate surface and the lower inner interface (between the first and the second layer).

Table 5. Normalised quantities, according to Equation (101), evaluated at $z_{(0)}$ and $z_{(1)}$ interfaces for laminate L using ZZT kinematics.

Model	$\overline{u}_1^{(k)}(0;\frac{b}{2})$	$\overline{u}_2^{(k)}(\frac{a}{2};0)$	$\overline{u}_3(\frac{a}{2};\frac{b}{2})$	$\overline{\sigma}_{11}^{(k)}(\frac{a}{2};\frac{b}{2})$	$\overline{\sigma}_{22}^{(k)}(\frac{a}{2};\frac{b}{2})$	$\overline{\tau}_{12}^{(k)}(0;0)$	$\overline{\tau}_{13}^{(k)}(0;\frac{b}{2})$	$\overline{\tau}_{23}^{(k)}(\frac{a}{2};0)$
				$z_{(0)}$ interface				
$ZZT^{(0,1)}$	6.5288	10.1027	0.7068	−0.5220	−0.0370	0.0261	2.6135	0.5713
$ZZT^{(0,N)}$	6.5288	10.1027	0.7068	−0.5220	−0.0370	0.0261	2.6135	0.5713
$ZZT^{(M0,M1)}$	6.5288	10.1027	0.7068	−0.5220	−0.0370	0.0261	2.6135	0.5713
				$z_{(1)}$ interface				
$ZZT^{(0,1)}$	2.2843	5.2656	0.7068	−0.1840	−0.4164	0.0119	2.6135	0.5713
$ZZT^{(0,N)}$	2.2843	5.2656	0.7068	−0.1840	−0.4164	0.0119	2.6135	0.5713
$ZZT^{(M0,M1)}$	2.2843	5.2656	0.7068	−0.1840	−0.4164	0.0119	2.6135	0.5713

Table 6. Normalised quantities, according to Equation (101), evaluated at $z_{(0)}$ and $z_{(1)}$ interfaces for laminate L using RZT kinematics.

Model	$\overline{u}_1^{(k)}(0;\frac{b}{2})$	$\overline{u}_2^{(k)}(\frac{a}{2};0)$	$\overline{u}_3(\frac{a}{2};\frac{b}{2})$	$\overline{\sigma}_{11}^{(k)}(\frac{a}{2};\frac{b}{2})$	$\overline{\sigma}_{22}^{(k)}(\frac{a}{2};\frac{b}{2})$	$\overline{\tau}_{12}^{(k)}(0;0)$	$\overline{\tau}_{13}^{(k)}(0;\frac{b}{2})$	$\overline{\tau}_{23}^{(k)}(\frac{a}{2};0)$
				$z_{(0)}$ interface				
$RZT^{(0,1)}$	6.8578	10.4824	0.7297	−0.5482	−0.0384	0.0272	1.7315	0.2090
$RZT^{(0,N)}$	6.8578	10.4824	0.7297	−0.5482	−0.0384	0.0272	1.7315	0.2090
$RZT^{(M0,M1)}$	6.8578	10.4824	0.7297	−0.5482	−0.0384	0.0272	1.7315	0.2090
				$z_{(1)}$ interface				
$RZT^{(0,1)}$	1.9929	5.0130	0.7297	−0.1609	−0.3963	0.0110	2.9903	1.4354
$RZT^{(0,N)}$	1.9929	5.0130	0.7297	−0.1609	−0.3963	0.0110	2.9903	1.4354
$RZT^{(M0,M1)}$	1.9929	5.0130	0.7297	−0.1609	−0.3963	0.0110	2.9903	1.4354

As expected, the results confirm the equivalency among the three scenarios adopted to characterise the through-the-thickness zigzag behaviour. Whereas the ZZT or RZT kinematics influence the model predictivity capabilities by giving different values between Tables 5 and 6, each methodology is able to compute the same values for displacements and stresses at the interfaces. The static equivalence of the three scenarios was numerically assessed; in the following examples, scenario 2 is adopted.

Figure 5 reports the displacement distribution across the laminate thickness.

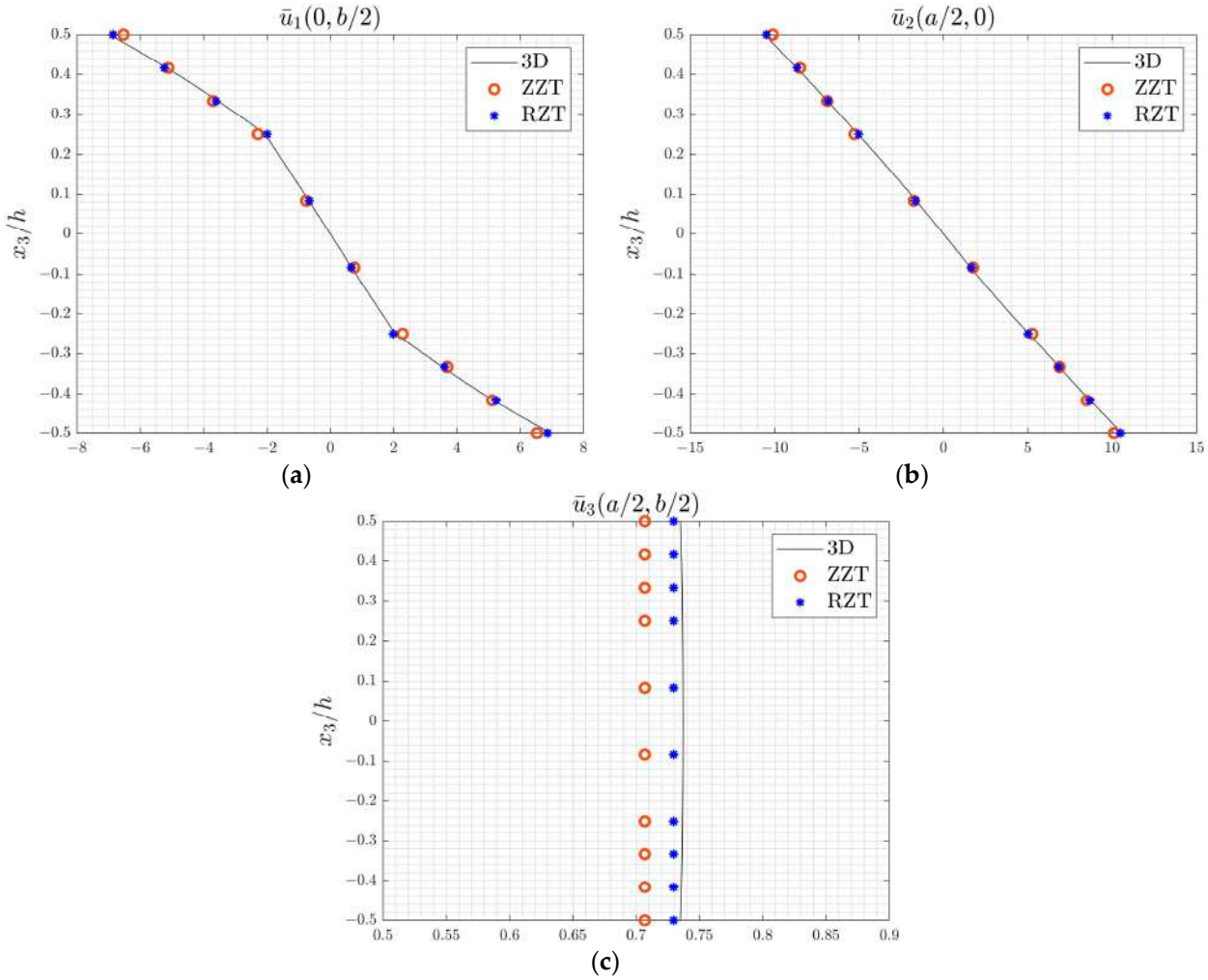

Figure 5. Through-the-thickness distributions of normalised displacements (**a**–**c**), according to Equation (101), for simply supported laminate L under bi-sinusoidal pressure.

It is interesting to observe very few differences in the in-plane displacement predictions between ZZT and RZT when compared with the three-dimensional solution computed using Pagano's solution [3]. On the other hand, the transverse displacement given by the ZZT model is less accurate than the RZT one since the transverse shear deformability is evaluated differently by the assumed kinematics.

Similarly, even Figures 6 and 7 suggest the same consideration. In fact, Figure 6 shows that both ZZT and RZT are accurate enough to match the three-dimensional behaviour well.

However, as reported in Table 5 and observable in Figure 7, the full enforcement of the transverse shear stress continuity across the laminate thickness leads to an overly stiff model. Relaxing the full transverse shear stress continuity by including an additional kinematic variable, as done in the RZT, results in a better prediction of the transverse shear plate behaviour.

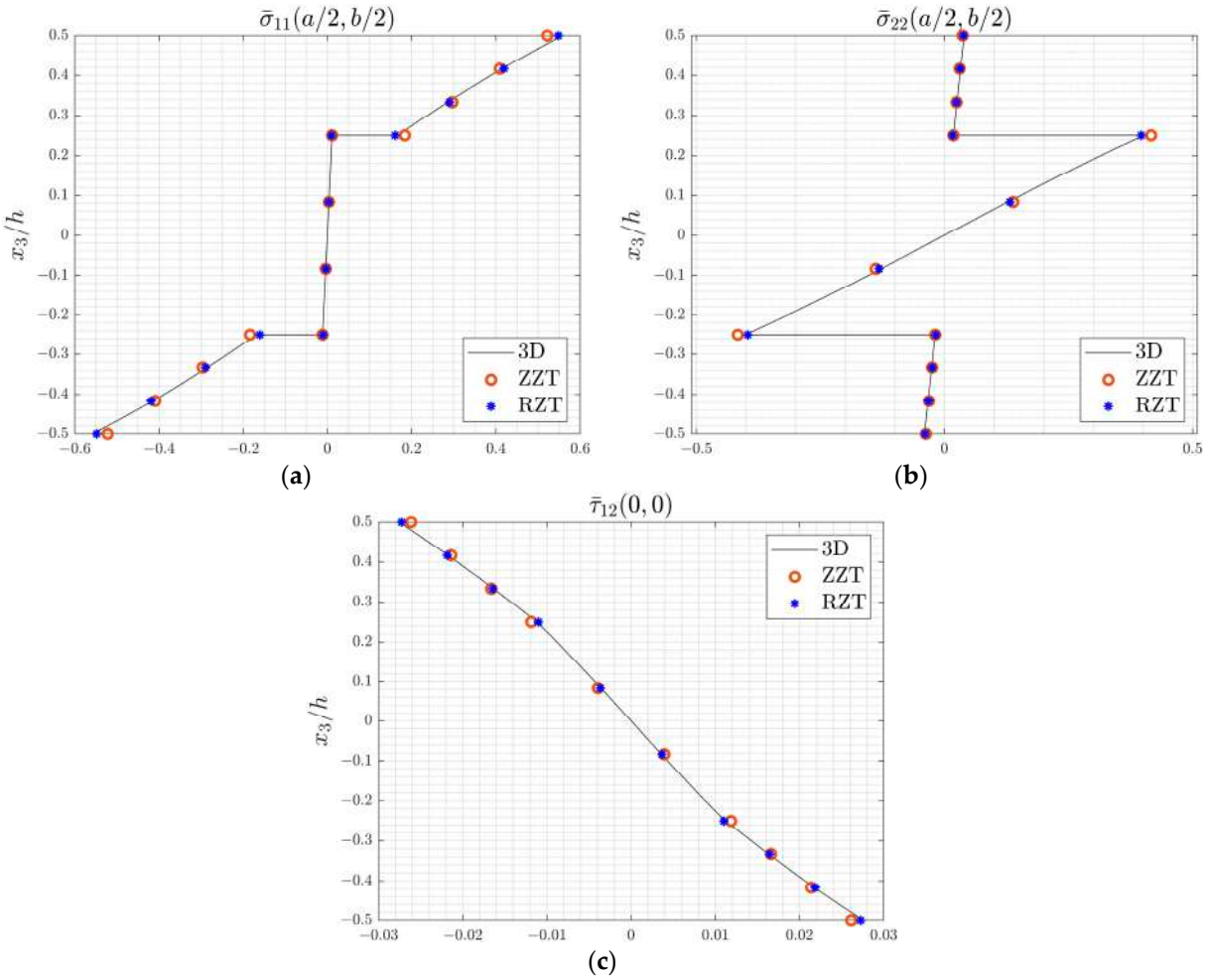

Figure 6. Through-the-thickness distributions of normalised in-plane stresses, according to Equation (101), for simply supported laminate L under bi-sinusoidal pressure (**a**–**c**).

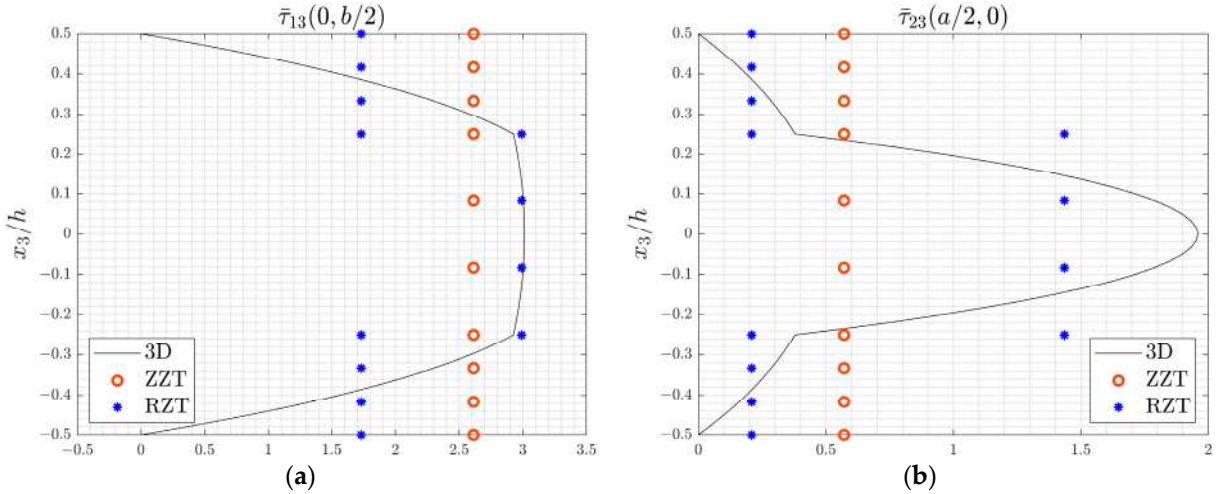

Figure 7. Through-the-thickness distributions of normalised transverse shear stresses, according to Equation (101), for simply supported laminate L under bi-sinusoidal pressure (**a**–**c**).

3.3. Free-Vibration Analysis

This example presents the dynamic equivalence among the presented methodologies to address the zigzag behaviour. The results for the first five normalised circular frequency are presented in Table 7.

Table 7. First five normalised, according to Equation (101), circular frequencies of simply supported laminate L using ZZT and RZT models.

Model	(1,1)	(1,2)	(2,1)	(2,2)	(1,3)
$ZZT^{(0,1)}$	37.44	74.82	86.29	108.76	139.92
$ZZT^{(0,N)}$	37.44	74.82	86.30	108.76	139.92
$ZZT^{(M0,M1)}$	37.44	74.82	86.30	108.76	139.92
$RZT^{(0,1)}$	36.86	69.10	85.32	104.25	119.23
$RZT^{(0,N)}$	36.86	69.10	85.32	104.25	119.23
$RZT^{(M0,M1)}$	36.86	69.10	85.32	104.25	119.23

As expected, differences between ZZT and RZT results are observable since the second model is slightly more deformable with respect to the first one. In addition, even for the modal case, the scenario characterising the zigzag in-plane distribution is not a discriminant of the model accuracy.

4. Conclusions

In this paper, new accomplishments on the equivalence of displacement-based first-order zigzag theories for the analysis of multilayered plates are presented. The fundamental ingredients of some of the first-order displacement-based zigzag Theories (ZZTs) are presented. Through a unified formulation, the in-plane local layer-wise contribution is characterised using different scenarios in which the full/partial transverse shear stress continuity at the layer interfaces is enforced for ZZTs/RZTs, respectively. The addressed scenarios and constraint conditions lead to a different description of the through-the-thickness distribution of the local in-plane displacement contribution; for each scenario, a detailed formulation and a final recursive formula are presented, highlighting the analogies and the differences. As demonstrated in the unified formulation, when the full/partial transverse shear stress continuity in the local in-plane characterisation is chosen, the zigzag theory or the refined zigzag theory can be easily obtained.

In a unified way, the governing equations and consistent boundary conditions have been derived using the d'Alembert principle.

The equivalence on the predictive capabilities of the considered scenarios is verified for each ZZT/RZT kinematics via numerical tests evaluating the global/local static and free-vibration behaviour of multilayered composite and sandwich plates. The provided numerical results substantiate the previous considerations on the equivalence of the predictivity capabilities of the investigated scenarios characterising the zigzag contribution. In fact, although different distributions could define the zigzag contribution according to a different set of constraint conditions (see Figures 3 and 4), the computed through-the-thickness displacements and stresses are exactly the same in each considered scenario. On the other hand, the model kinematics and the transverse shear stress continuity that differentiate the formulation of the ZZT model with respect to the RZT one are the sole discriminants of the model's accuracy.

In conclusion, this work wants to clarify some important aspects that characterise a zigzag model based on enforcing the transverse shear stress continuity. With particular attention placed on the ZZT/RZT kinematics, the generality of the proposed unified formulation offers researchers a solid mathematical background in the displacement-based first-order zigzag theory framework for analysing multilayered composite and sandwich plates, promoting further study in complex, innovative, lightweight structures. In addition, from a general point of view, and in light of the results reported in the available literature,

the RZT seems to perform better than the ZZT (e.g., more accuracy in transverse shear stress distribution at clamped edges and C^0-continuity requirements in FE formulations), despite a greater number of kinematic variables (e.g., for plates, five unknown variables for ZZT and seven for RZT).

This study and its final considerations hold for first-order displacement-based zigzag theories. As mentioned in the Introduction, higher-order contributions to the in-plane displacements and/or transverse displacements are often considered to evaluate the response of multilayered composite and sandwich structures, especially in the case of thick structures. Additionally, future perspectives in this sense are to extend this unified formulation by incorporating higher-order zigzag theories and a more complete review study that covers the existing RZT-based models and the numerical results.

Author Contributions: Conceptualisation, methodology, M.D.S. and M.S.; software, M.S.; validation and formal analysis, M.D.S. and M.S.; investigation, M.D.S. and M.S.; resources, M.S.; data curation, M.S.; writing—original draft preparation, writing—review and editing, visualisation, M.D.S. and M.S. All authors have read and agreed to the published version of the manuscript.

Funding: This research received no external funding.

Data Availability Statement: The data presented in this research study are available upon request from the corresponding author M. Sorrenti at matteo.sorrenti@polito.it.

Conflicts of Interest: The authors declare no conflicts of interest.

Appendix A

In this appendix, the second form of Equation (35), here recalled for brevity, is further elaborated in order to obtain a recursive form.

$$\boldsymbol{\gamma}^{L(k+1)} = \left(\mathbf{I} + \mathbf{A}^{(k+1,k)}\right)\boldsymbol{\gamma}^{L(k)} + \mathbf{A}^{(k+1,k)}\boldsymbol{\gamma}^{G}_{(0)} \tag{A1}$$

Let us make Equation (A1) explicit for some values of k:

$$\begin{aligned} k=1): \boldsymbol{\gamma}^{L(2)} &= \left(\mathbf{I} + \mathbf{A}^{(2,1)}\right)\boldsymbol{\gamma}^{L(1)} + \mathbf{A}^{(2,1)}\boldsymbol{\gamma}^{G}_{(0)} \\ &= \mathbf{a}^{L(2)}\boldsymbol{\gamma}^{L(1)} + \mathbf{a}^{(2)}\boldsymbol{\gamma}^{G}_{(0)} \\ k=2): \boldsymbol{\gamma}^{L(3)} &= \left(\mathbf{I} + \mathbf{A}^{(3,2)}\right)\boldsymbol{\gamma}^{L(2)} + \mathbf{A}^{(3,2)}\boldsymbol{\gamma}^{G}_{(0)} \end{aligned} \tag{A2}$$

Substituting the expression of $\boldsymbol{\gamma}^{L(2)}$ and collecting terms multiplied by $\boldsymbol{\gamma}^{L(1)}$ and $\boldsymbol{\gamma}^{G}_{(0)}$ yields

$$\boldsymbol{\gamma}^{L(3)} = \mathbf{a}^{L(3)}\boldsymbol{\gamma}^{L(1)} + \mathbf{a}^{(3)}\boldsymbol{\gamma}^{G}_{(0)} \tag{A3}$$

with

$$\begin{aligned} \mathbf{a}^{(3)} &= \left(\mathbf{I} + \mathbf{A}^{(3,2)}\right)\mathbf{a}^{(2)} + \mathbf{A}^{(3,2)} \\ \mathbf{a}^{L(3)} &= \left(\mathbf{I} + \mathbf{A}^{(3,2)}\right)\left(\mathbf{I} + \mathbf{a}^{(2)}\right) \end{aligned} \tag{A4}$$

Using the same approach for other values, Equation (A1) can be rewritten in the following recursive form:

$$\boldsymbol{\gamma}^{L(k+1)} = \mathbf{a}^{L(k+1)}\boldsymbol{\gamma}^{L(1)} + \mathbf{a}^{(k+1)}\boldsymbol{\gamma}^{G}_{(0)} \tag{A5}$$

with

$$\begin{aligned} \mathbf{a}^{(k+1)} &= \left(\mathbf{I} + \mathbf{A}^{(k+1,k)}\right)\mathbf{a}^{(k)} + \mathbf{A}^{(k+1,k)} \\ \mathbf{a}^{L(k+1)} &= \left(\mathbf{I} + \mathbf{A}^{(k+1,k)}\right)\left(\mathbf{I} + \mathbf{a}^{(k)}\right) \\ \mathbf{a}^{(1)} &= \mathbf{0} \end{aligned} \tag{A6}$$

Appendix B

In this appendix, let us demonstrate that the expression for $\boldsymbol{\beta}^{(k)}$ values given in Equation (56) is equivalent to that obtained for the en-RZT (see Ref. [34]).

Let us write Equation (56) for $k = 1$:

$$\mathbf{a}^{(1)}_{ZZT^{(0,N)}} = \boldsymbol{\beta}^{(1)} = -\frac{1}{h}\overline{\mathbf{S}}_t^{(1)}\mathbf{G} \tag{A7}$$

Substituting Equation (37) into the second form of Equation (41) yields

$$\begin{aligned} &\mathbf{a}^{(1)} = \mathbf{0} \\ &\mathbf{a}^{(p)} = \mathbf{a}^{(p-1)} + \left(\overline{\mathbf{S}}_t^{(p)}\overline{\mathbf{Q}}_t^{(p-1)} - \mathbf{I}\right)\left(\mathbf{I} + \mathbf{a}^{(p-1)}\right) \\ &= \overline{\mathbf{S}}_t^{(p)}\overline{\mathbf{Q}}_t^{(p-1)} + \overline{\mathbf{S}}_t^{(p)}\overline{\mathbf{Q}}_t^{(p-1)}\mathbf{a}^{(p-1)} - \mathbf{I} \;\; (p = 2, \ldots, N) \end{aligned} \tag{A8}$$

Using Equation (A8) for $\mathbf{a}^{(p)}$ in the second expression of Equation (52) yields

$$\begin{aligned} \mathbf{a} &= \sum_{p=2}^{N} h^{(p)}\mathbf{a}^{(p)} = \sum_{p=2}^{N} h^{(p)}\left(\overline{\mathbf{S}}_t^{(p)}\overline{\mathbf{Q}}_t^{(p-1)} + \overline{\mathbf{S}}_t^{(p)}\overline{\mathbf{Q}}_t^{(p-1)}\mathbf{a}^{(p-1)} - \mathbf{I}\right) \\ &= \mathbf{I}\left(-h + h^{(1)}\right) + \sum_{p=2}^{N} h^{(p)}\overline{\mathbf{S}}_t^{(p)}\overline{\mathbf{Q}}_t^{(p-1)} + \sum_{p=2}^{N} h^{(p)}\overline{\mathbf{S}}_t^{(p)}\overline{\mathbf{Q}}_t^{(p-1)}\mathbf{a}^{(p-1)} \end{aligned} \tag{A9}$$

Now, let us focus on the term in Equation (A9),

$$\mathbf{I}h^{(1)} + \sum_{p=2}^{N} h^{(p)}\overline{\mathbf{S}}_t^{(p)}\overline{\mathbf{Q}}_t^{(p-1)} + \sum_{p=2}^{N} h^{(p)}\overline{\mathbf{S}}_t^{(p)}\overline{\mathbf{Q}}_t^{(p-1)}\mathbf{a}^{(p-1)} \tag{A10}$$

Expanding Equation (A8), it can be observed that

$$\mathbf{a}^{(p)} = -\mathbf{I} + \overline{\mathbf{S}}_t^{(p)}\overline{\mathbf{Q}}_t^{(1)} \;\; (p = 2, \ldots, N) \tag{A11}$$

Using Equation (A11) in Equation (A10), we obtain

$$\begin{aligned} &\sum_{p=2}^{N} h^{(p)}\overline{\mathbf{S}}_t^{(p)}\overline{\mathbf{Q}}_t^{(p-1)}\mathbf{a}^{(p-1)} = \sum_{p=2}^{N} h^{(p)}\overline{\mathbf{S}}_t^{(p)}\overline{\mathbf{Q}}_t^{(p-1)}\left(-\mathbf{I} + \overline{\mathbf{S}}_t^{(p)}\overline{\mathbf{Q}}_t^{(1)}\right) \\ &= \sum_{p=2}^{N}\left(-h^{(p)}\overline{\mathbf{S}}_t^{(p)}\overline{\mathbf{Q}}_t^{(p-1)} + h^{(p)}\overline{\mathbf{S}}_t^{(p)}\overline{\mathbf{Q}}_t^{(1)}\right) \end{aligned} \tag{A12}$$

Thus, taking into account that $h^{(1)}\mathbf{I} = h^{(1)}\overline{\mathbf{S}}_t^{(1)}\overline{\mathbf{Q}}_t^{(1)}$, we can write

$$\begin{aligned} &h^{(1)}\overline{\mathbf{S}}_t^{(1)}\overline{\mathbf{Q}}_t^{(1)} + \sum_{p=2}^{N} h^{(p)}\overline{\mathbf{S}}_t^{(p)}\overline{\mathbf{Q}}_t^{(p-1)} + \sum_{p=2}^{N}\left(-h^{(p)}\overline{\mathbf{S}}_t^{(p)}\overline{\mathbf{Q}}_t^{(p-1)} + h^{(p)}\overline{\mathbf{S}}_t^{(p)}\overline{\mathbf{Q}}_t^{(1)}\right) \\ &= \left(\sum_{p=1}^{N} h^{(p)}\overline{\mathbf{S}}_t^{(p)}\right)\overline{\mathbf{Q}}_t^{(1)} = \overline{\mathbf{S}}_t\overline{\mathbf{Q}}_t^{(1)} \end{aligned} \tag{A13}$$

Substituting Equation (A13) into Equation (A9) yields

$$\mathbf{a} = -h\mathbf{I} + \overline{\mathbf{S}}_t\overline{\mathbf{Q}}_t^{(1)} \tag{A14}$$

Remembering the definition of $\overline{\mathbf{S}}_t$ as function of the $\mathbf{G}$ matrix (see Equation (53)), we can write the following equivalence:

$$\overline{\mathbf{S}}_t\overline{\mathbf{Q}}_t^{(1)} = h\left(\overline{\mathbf{S}}_t^{(1)}\mathbf{G}\right)^{-1} \tag{A15}$$

Finally, adopting Equations (A11), (A14) and (A15) in Equation (56) yields

$$\begin{aligned}\mathbf{a}^{(k)}_{ZZT^{(0,N)}} &= -\mathbf{I} + \overline{\mathbf{S}}_t^{(k)}\overline{\mathbf{Q}}_t^{(1)} - \tfrac{1}{h}\overline{\mathbf{S}}_t^{(k)}\mathbf{G} = -\mathbf{I} + \overline{\mathbf{S}}_t^{(k)}\overline{\mathbf{Q}}_t^{(1)} - \tfrac{1}{h}\overline{\mathbf{S}}_t^{(k)}\mathbf{G}\left(-h\mathbf{I} + \overline{\mathbf{S}}_t\overline{\mathbf{Q}}_t^{(1)}\right) \\ &= -\mathbf{I} + \overline{\mathbf{S}}_t^{(k)}\overline{\mathbf{Q}}_t^{(1)} + \overline{\mathbf{S}}_t^{(k)}\mathbf{G} - \tfrac{1}{h}\overline{\mathbf{S}}_t^{(k)}\mathbf{G}\overline{\mathbf{S}}_t\overline{\mathbf{Q}}_t^{(1)} \\ &= \overline{\mathbf{S}}_t^{(k)}\mathbf{G} - \mathbf{I}(k = 1, \ldots, N)\end{aligned} \tag{A16}$$

i.e., Equation (A16) is the same expression for $\boldsymbol{\beta}^{(k)}$ of the en-RZT.

Appendix C

This appendix reports the main steps for obtaining the plate's governing equations, i.e., Equations (95)–(98), and boundary conditions, i.e., Equation (99). Moreover, it reports the expressions of the plate's constitutive relations.

Let us recall some mathematical properties of the *del operator* ∇. As well as all matrices of differential operators, it has some of the properties of a matrix; however, it does not follow the commutative and associative rules of matrix multiplication. Let us consider the vector $\mathbf{q}$ whose elements q_i are the Cartesian components of the vector, which are functions of the space variable $\mathbf{X}$; thus,

$$\left(\nabla^T\mathbf{q}\right)^T = q_{i,i} \neq \mathbf{q}^T\nabla = q_i(\cdot)_{,i} \tag{A17}$$

In fact, $\nabla^T\mathbf{q}$ is the divergence of $\mathbf{q}$, whereas $\mathbf{q}^T\nabla$ is a scalar differential operator. Furthermore, $\mathbf{q}^T(\nabla\mathbf{B}) \neq (\mathbf{q}^T\nabla)\mathbf{B}$. Let us introduce the following convention: When ∇ operates on a vector field, an arrow above pointing to the right $(\rightarrow)$ means that it multiplies the vector field to its right (right multiplication); an arrow above pointing to the left $(\leftarrow)$ means that it multiplies the vector field to its left (left multiplication). So, the following rule for the transpose of the product holds: $\left(\overrightarrow{\nabla}^T\mathbf{q}\right) = \mathbf{q}^T\overleftarrow{\nabla} = q_{i,i}$.

Using the introduced notation, the integration by parts may be written as follows:

$$\int_\Omega \mathbf{q}^T\delta\overrightarrow{\nabla}(\cdot)d\Omega = -\int_\Omega \mathbf{q}^T\overleftarrow{\nabla}\delta(\cdot)d\Omega + \int_\Gamma \mathbf{q}^T\nabla_n\delta(\cdot)d\Gamma \tag{A18}$$

where ∇_n is formally obtained by substituting $(\cdot)_{,\alpha}$ in ∇ with $n_\alpha(\alpha = 1, 2)$, the direction cosines of the outward unit normal n to Γ with respect to the α-axis; (n, s, x_3) forms a right-handed coordinate system, with s being the unit vector tangent to Γ.

Let us further specify some of the terms that appear in the governing functional, i.e., Equation (92),

$$\overset{\sim}{\mathbf{E}}_p^{(k)} = \begin{Bmatrix}\widetilde{u}^{G(k)}_{1,1}\\ \widetilde{u}^{G(k)}_{1,2}\\ \widetilde{u}^{G(k)}_{2,1}\\ \widetilde{u}^{G(k)}_{2,2}\end{Bmatrix} + \begin{Bmatrix}\widetilde{u}^{L(k)}_{1,1}\\ \widetilde{u}^{L(k)}_{1,2}\\ \widetilde{u}^{L(k)}_{2,1}\\ \widetilde{u}^{L(k)}_{2,2}\end{Bmatrix} = \begin{Bmatrix}\overset{\sim}{\mathbf{E}}{}^{G(k)}_{p1}\\ \overset{\sim}{\mathbf{E}}{}^{G(k)}_{p2}\end{Bmatrix} + \begin{Bmatrix}\overset{\sim}{\mathbf{E}}{}^{L(k)}_{p1}\\ \overset{\sim}{\mathbf{E}}{}^{L(k)}_{p2}\end{Bmatrix} = \overset{\sim}{\mathbf{E}}{}_p^{G(k)} + \overset{\sim}{\mathbf{E}}{}_p^{L(k)} \tag{A19}$$

where

$$\begin{aligned}&\overset{\sim}{\mathbf{E}}{}^{G(k)}_{p\alpha} = \nabla u^{(0)}_\alpha + x_3\nabla\theta_\alpha = \mathbf{E}_{m\alpha} + x_3\mathbf{E}_{\theta\alpha} \\ &\overset{\sim}{\mathbf{E}}{}^{L(k)}_{p\alpha} = \nabla u^{L(k)}_\alpha = \left(\varphi^{(k)}_{\alpha\beta} + \kappa_{M0M1}C^{(0)}_{\mu\alpha\beta}\right)\left(\kappa_{ZZT}\mathbf{E}_{\gamma\beta} + \kappa_{RZT}\mathbf{E}_{\psi\beta}\right)\ \ \beta = 1, 2 \\ &\mathbf{E}_{\gamma\alpha} = \nabla\left(\theta_\alpha + \mu^{(0)}_{3,\alpha}\right) = \mathbf{E}_{\theta\alpha} + \nabla\mu^{(0)}_{3,\alpha};\ \mathbf{E}_{\gamma\alpha} = \nabla\psi_\alpha\end{aligned} \tag{A20}$$

Moreover,

$$\boldsymbol{\varphi}^{(k)}(x_3) = \begin{bmatrix} \varphi_{11}(x_3) & \varphi_{12}(x_3) \\ \varphi_{21}(x_3) & \varphi_{22}(x_3) \end{bmatrix}^{(k)}; \mathbf{C}_u^{(0)} = \begin{bmatrix} C_{u11}^{(0)} & C_{u12}^{(0)} \\ C_{u21}^{(0)} & C_{u22}^{(0)} \end{bmatrix} \tag{A21}$$

Substituting Equations (A19)–(A21) and Equations (22) and (24) into Equation (92) yields

$$\int_\Omega \left\langle \tilde{\boldsymbol{\sigma}}_{p\alpha}^{(k)T} \delta \tilde{\mathbf{E}}_{p\alpha}^{G(k)} \right\rangle d\Omega = \int_\Omega \left\langle \tilde{\boldsymbol{\sigma}}_{p\alpha}^{(k)T} \delta(\mathbf{E}_{m\alpha} + x_3 \mathbf{E}_{\theta\alpha}) \right\rangle d\Omega = \int_\Omega \mathbf{N}_\alpha^T \delta \mathbf{E}_{m\alpha} d\Omega + \int_\Omega \mathbf{M}_\alpha^T \delta \mathbf{E}_{\theta\alpha} d\Omega \tag{A22}$$

$$\begin{aligned} &\int_\Omega \left\langle \tilde{\boldsymbol{\sigma}}_{p\alpha}^{(k)T} \delta \tilde{\mathbf{E}}_{p\alpha}^{L(k)} \right\rangle d\Omega = \int_\Omega \left\langle \tilde{\boldsymbol{\sigma}}_{p\alpha}^{(k)T} \left(\varphi_{\alpha\beta}^{(k)} + \kappa_{M0M1} C_{u\alpha\beta}^{(0)} \right) \left(\kappa_{ZZT} \delta \mathbf{E}_{\gamma\beta} + \kappa_{RZT} \delta \mathbf{E}_{\psi\beta} \right) \right\rangle d\Omega \\ &= \int_\Omega \left(\mathbf{M}_\alpha^{\phi T} + \mathbf{M}_\alpha^{CT} \right) \left(\kappa_{ZZT} \delta \mathbf{E}_{\gamma\alpha} + \kappa_{RZT} \delta \mathbf{E}_{\psi\alpha} \right) d\Omega \end{aligned} \tag{A23}$$

where

$$\begin{aligned} &(\mathbf{N}_\alpha, \mathbf{M}_\alpha) = \left\langle (1, x_3) \tilde{\boldsymbol{\sigma}}_{p\alpha}^{(k)} \right\rangle; \\ &\left(\mathbf{M}_\alpha^\phi, \mathbf{M}_\alpha^C \right) = \left\langle \left(\varphi_{\beta\alpha}^{(k)}, \kappa_{M0M1} C_{u\beta\alpha}^{(0)} \right) \tilde{\boldsymbol{\sigma}}_{p\alpha}^{(k)} \right\rangle = \left(\left\langle \varphi_{\beta\alpha}^{(k)} \tilde{\boldsymbol{\sigma}}_{p\alpha}^{(k)} \right\rangle, \kappa_{M0M1} C_{u\beta\alpha}^{(0)} \mathbf{N}_\alpha \right) \quad \beta = 1, 2 \end{aligned} \tag{A24}$$

Furthermore,

$$\int_\Omega \left\langle \tilde{\boldsymbol{\sigma}}_t^{(k)T} \delta \tilde{\boldsymbol{\gamma}}_t^{(k)} \right\rangle d\Omega = \int_\Omega \mathbf{Q}^T \delta \boldsymbol{\gamma}_{(0)}^G d\Omega + \int_\Omega \mathbf{Q}^{\phi T} \left(\kappa_{ZZT} \delta \boldsymbol{\gamma}_{(0)}^G + \kappa_{RZT} \delta \boldsymbol{\psi} \right) d\Omega \tag{A25}$$

where

$$\left(\mathbf{Q}, \mathbf{Q}^\phi \right) = \left\langle \left(\mathbf{I}, \boldsymbol{\beta}^{(k)T} \right) \tilde{\boldsymbol{\sigma}}_t^{(k)} \right\rangle \tag{A26}$$

Integrating Equations (A22), (A23) and (A25) by parts and remembering Equation (A20) and the following relation on the boundary Γ:

$$\begin{aligned} &(\cdot)_{\alpha n} = n_\beta (\cdot)_{\alpha\beta}; \;\; (\cdot)_n = n_\alpha (\cdot)_{\alpha n}; \;\; (\cdot)_{ns} = n_1 (\cdot)_{2n} - n_2 (\cdot)_{1n}; \\ &(\cdot)_n = n_1 (\cdot)_{,1} - n_2 (\cdot)_{,2}; \;\; (\cdot)_s = n_1 (\cdot)_{,2} - n_2 (\cdot)_{,1} \end{aligned} \tag{A27}$$

we obtain

$$\begin{aligned} &\int_\Omega \mathbf{N}_\alpha^T \delta \mathbf{E}_{m\alpha} d\Omega = -\int_\Omega \mathbf{N}_\alpha^T \overleftarrow{\nabla} \delta u_\alpha^{(0)} d\Omega + \oint_\Gamma \left(N_n \delta u_n^{(0)} + N_s \delta u_s^{(0)} \right) d\Gamma \\ &\int_\Omega \mathbf{M}_\alpha^T \delta \mathbf{E}_{\theta\alpha} d\Omega = -\int_\Omega \mathbf{M}_\alpha^T \overleftarrow{\nabla} \delta \theta_\alpha d\Omega + \oint_\Gamma \left(M_n \delta \theta_n + N_s \delta \theta_s \right) d\Gamma \\ &\int_\Omega \left(\mathbf{M}_\alpha^{\phi T} + \mathbf{M}_\alpha^{CT} \right) \left(\kappa_{ZZT} \delta \mathbf{E}_{\gamma\alpha} + \kappa_{RZT} \delta \mathbf{E}_{\psi\alpha} \right) d\Omega \\ &= -\int_\Omega \underline{\left(\mathbf{M}_\alpha^{\phi T} + \mathbf{M}_\alpha^{CT} \right) \overleftarrow{\nabla}} \left(\kappa_{ZZT} \left(\delta \theta_\alpha + \underline{\delta u_{3,\alpha}^{(0)}} \right) + \kappa_{RZT} \delta \psi_\alpha \right) d\Omega \\ &+ \oint_\Gamma \left(M_n^\phi + M_n^C \right) \left(\kappa_{ZZT} \left(\delta \theta_n + \delta u_{3,n}^{(0)} \right) + \kappa_{RZT} \delta \psi_n \right) d\Gamma \\ &+ \oint_\Gamma \left(M_s^\phi + M_s^C \right) \left(\kappa_{ZZT} \delta \theta_s + \kappa_{RZT} \delta \psi_s \right) d\Gamma - \oint_\Gamma \left(M_s^\phi + M_s^C \right)_{,s} \delta u_3^{(0)} d\Gamma \\ &\int_\Omega \mathbf{Q}^T \delta \boldsymbol{\gamma}_{(0)}^G d\Omega = \int_\Omega Q_\alpha \delta \theta_\alpha d\Omega - \int_\Omega \mathbf{Q}^T \overleftarrow{\nabla} \delta u_3^{(0)} d\Omega + \oint_\Gamma V_3 \delta u_3^{(0)} d\Gamma \\ &\int_\Omega \left(\mathbf{Q}^{\phi T} \delta \boldsymbol{\gamma}_{(0)}^G \right) d\Omega = \int_\Omega Q_\alpha^\phi \delta \theta_\alpha d\Omega - \int_\Omega \mathbf{Q}^{\phi T} \overleftarrow{\nabla} \delta u_3^{(0)} d\Omega + \oint_\Gamma V_3^\phi \delta u_3^{(0)} d\Gamma \\ &\int_\Omega \mathbf{Q}^{\phi T} \delta \boldsymbol{\psi} d\Omega = \int_\Omega Q_\alpha^\phi \delta \psi_\alpha d\Omega \end{aligned} \tag{A28}$$

where $\left(V_3, V_3^{\phi}\right) = \left(\mathbf{Q}^T, \mathbf{Q}^{\phi T}\right)\nabla_n$. Elaborating the underlined term in Equation (A28) further yields

$$\int_{\Omega} \kappa_{ZZT}\left(\left(\mathbf{M}_{\alpha}^{\phi T} + \mathbf{M}_{\alpha}^{CT}\right)\overleftarrow{\nabla}\right)_{,\alpha} \delta u_3^{(0)} d\Omega - \kappa_{ZZT}\oint_{\Gamma} n_{\alpha}\left(\left(\mathbf{M}_{\alpha}^{\phi T} + \mathbf{M}_{\alpha}^{CT}\right)\overleftarrow{\nabla}\right)\delta u_3^{(0)} d\Gamma \tag{A29}$$

with

$$\begin{aligned} &n_{\alpha}\left(\left(\mathbf{M}_{\alpha}^{\phi T} + \mathbf{M}_{\alpha}^{CT}\right)\overleftarrow{\nabla}\right) = M_{\alpha n,\alpha}^{\phi} + M_{\alpha n,\alpha}^{C} = M_{n,n}^{\phi} + M_{n,n}^{C} + M_{s,s}^{\phi} + M_{s,s}^{C} \\ &M_{\alpha n}^{\phi} = n_{\beta} M_{\beta\alpha}^{\phi} \end{aligned} \tag{A30}$$

Let us consider now the virtual variation in the work done by the inertia forces, i.e., Equation (93); we can write

$$\begin{aligned} \delta W_{in} = -\int_{\Omega} &\left\langle \rho^{(k)}\left(\ddot{\mathbf{u}}^{(0)} + x_3\ddot{\boldsymbol{\theta}} + \left(\boldsymbol{\varphi}^{(k)} + \kappa_{M0M1}\mathbf{C}_u^{(0)}\right)\left(\kappa_{ZZT}\ddot{\boldsymbol{\gamma}}_{(0)}^{G} + \kappa_{RZT}\ddot{\boldsymbol{\psi}}\right)\right)^T \right. \\ &\left. \cdot\,\delta\left(\mathbf{u}^{(0)} + x_3\boldsymbol{\theta} + \left(\boldsymbol{\varphi}^{(k)} + \kappa_{M0M1}\mathbf{C}_u^{(0)}\right)\left(\kappa_{ZZT}\boldsymbol{\gamma}_{(0)}^{G} + \kappa_{RZT}\boldsymbol{\psi}\right)\right) + \rho^{(k)}\ddot{u}_3^{(0)}\delta u_3^{(0)}\right\rangle d\Omega \\ = \delta W_{in1} + \delta W_{in2} + \delta W_{in3} + \delta W_{in4} \end{aligned} \tag{A31}$$

where

$$\begin{aligned} \delta W_{in1} &= -\int_{\Omega}\left(m^{(0)}\ddot{\mathbf{u}}^{(0)} + m^{(1)}\ddot{\boldsymbol{\theta}} + \left(\mathbf{m}^{\phi(0)} + \mathbf{m}^{C(0)}\right)\left(\kappa_{ZZT}\ddot{\boldsymbol{\theta}} + \kappa_{RZT}\ddot{\boldsymbol{\psi}}\right)\right. \\ &\left. + \left(\kappa_{ZZT}\left(\mathbf{m}^{\phi(0)} + \mathbf{m}^{C(0)}\right)\nabla\ddot{u}_3^{(0)}\right)\right)^T \delta\mathbf{u}^{(0)} d\Omega \\ &= -\int_{\Omega}\left(m^{(0)}\ddot{u}_{\alpha}^{(0)} + m^{(1)}\ddot{\theta}_{\alpha} + \left(m_{\alpha\beta}^{\phi(0)} + m_{\alpha\beta}^{C(0)}\right)\left(\kappa_{ZZT}\ddot{\theta}_{\beta} + \kappa_{RZT}\ddot{\psi}_{\beta}\right)\right. \\ &\left. + \left(\kappa_{ZZT}\left(m_{\alpha\beta}^{\phi(0)} + m_{\alpha\beta}^{C(0)}\right)\nabla\ddot{u}_{3,\beta}^{(0)}\right)\right)^T \delta u_{\alpha}^{(0)} d\Omega \end{aligned} \tag{A32}$$

$$\begin{aligned} \delta W_{in2} &= -\int_{\Omega}\left(m^{(1)}\ddot{\mathbf{u}}^{(0)} + m^{(2)}\ddot{\boldsymbol{\theta}} + \left(\mathbf{m}^{\phi(1)} + \mathbf{m}^{C(1)}\right)\left(\kappa_{ZZT}\ddot{\boldsymbol{\theta}} + \kappa_{RZT}\ddot{\boldsymbol{\psi}}\right)\right. \\ &\left. + \left(\kappa_{ZZT}\left(\mathbf{m}^{\phi(1)} + \mathbf{m}^{C(1)}\right)\nabla\ddot{u}_3^{(0)}\right)\right)^T \delta\boldsymbol{\theta} d\Omega \\ &= -\int_{\Omega}\left(m^{(1)}\ddot{u}_{\alpha}^{(0)} + m^{(2)}\ddot{\theta}_{\alpha} + \left(m_{\alpha\beta}^{\phi(1)} + m_{\alpha\beta}^{C(1)}\right)\left(\kappa_{ZZT}\ddot{\theta}_{\beta} + \kappa_{RZT}\ddot{\psi}_{\beta}\right)\right. \\ &\left. + \left(\kappa_{ZZT}\left(m_{\alpha\beta}^{\phi(1)} + m_{\alpha\beta}^{C(1)}\right)\nabla\ddot{u}_{3,\beta}^{(0)}\right)\right)^T \delta\theta_{\alpha} d\Omega \end{aligned} \tag{A33}$$

$$\begin{aligned} \delta W_{in3} = -\int_{\Omega}\Bigg(&\left(\mathbf{m}^{\phi(0)} + \mathbf{m}^{C(0)}\right)^T\ddot{\mathbf{u}}^{(0)} + \left(\mathbf{m}^{\phi(1)} + \mathbf{m}^{C(1)}\right)^T\ddot{\boldsymbol{\theta}} \\ &+\kappa_{ZZT}\left(\mathbf{m}^{\phi\phi(0)} + \mathbf{m}^{\phi c(0)} + \mathbf{m}^{C\phi(0)} + \mathbf{m}^{CC(0)}\right)^T\ddot{\boldsymbol{\gamma}}_{(0)}^{G}\Bigg)\kappa_{ZZT}\delta\boldsymbol{\theta} \\ &+\Bigg(\left(\mathbf{m}^{\phi(0)} + \mathbf{m}^{C(0)}\right)^T\ddot{\mathbf{u}}^{(0)} + \left(\mathbf{m}^{\phi(1)} + \mathbf{m}^{C(1)}\right)^T\ddot{\boldsymbol{\theta}} \\ &+\kappa_{RZT}\left(\mathbf{m}^{\phi\phi(0)} + \mathbf{m}^{\phi c(0)} + \mathbf{m}^{C\phi(0)} + \mathbf{m}^{CC(0)}\right)^T\ddot{\boldsymbol{\psi}}\Bigg)\kappa_{RZT}\delta\ddot{\boldsymbol{\psi}} \\ &+\Bigg(\left(\mathbf{m}^{\phi(0)} + \mathbf{m}^{C(0)}\right)^T\ddot{\mathbf{u}}^{(0)} + \left(\mathbf{m}^{\phi(1)} + \mathbf{m}^{C(1)}\right)^T\ddot{\boldsymbol{\theta}} \\ &+\kappa_{ZZT}\left(\mathbf{m}^{\phi\phi(0)} + \mathbf{m}^{\phi c(0)} + \mathbf{m}^{C\phi(0)} + \mathbf{m}^{CC(0)}\right)^T\ddot{\boldsymbol{\gamma}}_{(0)}^{G}\Bigg)\kappa_{ZZT}\delta\nabla\ddot{u}_3^{(0)} d\Omega \end{aligned} \tag{A34}$$

$$\delta W_{in4} = -\int_{\Omega} m^{(0)}\ddot{u}_3^{(0)}\delta u_3^{(0)} d\Omega \tag{A35}$$

where the inertia resultants that appear in Equations (A31)–(A34) are defined as follows:

$$\begin{aligned}
&\left(m^{(0)}, m^{(1)}, m^{(2)}\right) = \left\langle \rho^{(k)}\left(1, x_3, x_3^2\right)\right\rangle; \left(\mathbf{m}^{\phi(0)}, \mathbf{m}^{\phi(1)}\right) = \left\langle \rho^{(k)}\boldsymbol{\varphi}^{(k)}(1, x_3)\right\rangle;\\
&\left(\mathbf{m}^{C(0)}, \mathbf{m}^{C(1)}\right) = \kappa_{M0M1}\left\langle \rho^{(k)}\mathbf{C}_u^{(0)}(1, x_3)\right\rangle;\\
&\left(\mathbf{m}^{\phi\phi(0)}, \mathbf{m}^{\phi C(0)}\right) = \left\langle \rho^{(k)}\boldsymbol{\varphi}^{(k)T}\left(\boldsymbol{\varphi}^{(k)}, \kappa_{M0M1}\mathbf{C}_u^{(0)}\right)\right\rangle;\\
&\left(\mathbf{m}^{C\phi(0)}, \mathbf{m}^{CC(0)}\right) = \kappa_{M0M1}\left\langle \rho^{(k)}\mathbf{C}_u^{(0)T}\left(\boldsymbol{\varphi}^{(k)}, \mathbf{C}_u^{(0)}\right)\right\rangle;
\end{aligned} \tag{A36}$$

Note that $\mathbf{m}^{C(0)} = m^{(0)}\mathbf{C}_u^{(0)}$.
Elaborating Equation (A34) further yields

$$\begin{aligned}
\delta W_{in3} = &-\int_\Omega \kappa_{ZZT}\Big(\left(\mathbf{m}^{\phi(0)} + \mathbf{m}^{C(0)}\right)^T\ddot{\mathbf{u}}^{(0)} + \left(\mathbf{m}^{\phi(1)} + \mathbf{m}^{C(1)}\right)^T\ddot{\boldsymbol{\theta}}\\
&+\kappa_{ZZT}\left(\mathbf{m}^{\phi\phi(0)} + \mathbf{m}^{\phi c(0)} + \mathbf{m}^{C\phi(0)} + \mathbf{m}^{CC(0)}\right)^T\ddot{\boldsymbol{\gamma}}_{(0)}^G\Big)\delta\boldsymbol{\theta}\\
&+\kappa_{RZT}\Big(\left(\mathbf{m}^{\phi(0)} + \mathbf{m}^{C(0)}\right)^T\ddot{\mathbf{u}}^{(0)} + \left(\mathbf{m}^{\phi(1)} + \mathbf{m}^{C(1)}\right)^T\ddot{\boldsymbol{\theta}}\\
&+\kappa_{RZT}\left(\mathbf{m}^{\phi\phi(0)} + \mathbf{m}^{\phi c(0)} + \mathbf{m}^{C\phi(0)} + \mathbf{m}^{CC(0)}\right)^T\ddot{\boldsymbol{\psi}}\Big)\delta\boldsymbol{\psi}\\
&-\kappa_{ZZT}\Big(\left(\mathbf{m}^{\phi(0)} + \mathbf{m}^{C(0)}\right)^T\ddot{\mathbf{u}}^{(0)} + \left(\mathbf{m}^{\phi(1)} + \mathbf{m}^{C(1)}\right)^T\ddot{\boldsymbol{\theta}}\\
&+\kappa_{ZZT}\left(\mathbf{m}^{\phi\phi(0)} + \mathbf{m}^{\phi c(0)} + \mathbf{m}^{C\phi(0)} + \mathbf{m}^{CC(0)}\right)^T\ddot{\boldsymbol{\gamma}}_{(0)}^G\Big)^T\overleftarrow{\nabla}\delta u_3^{(0)}d\Omega\\
&+\kappa_{ZZT}\oint_\Gamma\Big(\left(\mathbf{m}^{\phi(0)} + \mathbf{m}^{C(0)}\right)^T\ddot{\mathbf{u}}^{(0)} + \left(\mathbf{m}^{\phi(1)} + \mathbf{m}^{C(1)}\right)^T\ddot{\boldsymbol{\theta}}\\
&+\left(\mathbf{m}^{\phi\phi(0)} + \mathbf{m}^{\phi C(0)} + \mathbf{m}^{C\phi(0)} + \mathbf{m}^{CC(0)}\right)^T\ddot{\boldsymbol{\gamma}}_{(0)}^G\Big)\nabla_n\delta u_3^{(0)}d\Gamma\\
= &-\int_\Omega \kappa_{ZZT}\Big(\left(m_{\beta\alpha}^{\phi(0)} + m_{\beta\alpha}^{C(0)}\right)\ddot{u}_\beta^{(0)} + \left(m_{\beta\alpha}^{\phi(1)} + m_{\beta\alpha}^{C(1)}\right)\ddot{\theta}_\beta\\
&+\kappa_{ZZT}\left(m_{\beta\alpha}^{\phi\phi(0)} + m_{\beta\alpha}^{\phi C(0)} + m_{\beta\alpha}^{C\phi(0)} + m_{\beta\alpha}^{CC(0)}\right)\left(\ddot{\theta}_\beta + \ddot{u}_{3,\beta}^{(0)}\right)\Big)\delta\theta_\alpha\\
&+\kappa_{RZT}\Big(\left(m_{\beta\alpha}^{\phi(0)} + m_{\beta\alpha}^{C(0)}\right)\ddot{u}_\beta^{(0)} + \left(m_{\beta\alpha}^{\phi(1)} + m_{\beta\alpha}^{C(1)}\right)\ddot{\theta}_\beta\\
&+\kappa_{RZT}\left(m_{\beta\alpha}^{\phi\phi(0)} + m_{\beta\alpha}^{\phi C(0)} + m_{\beta\alpha}^{C\phi(0)} + m_{\beta\alpha}^{CC(0)}\right)\ddot{\psi}_\beta\Big)\delta\psi_\alpha\\
&-\kappa_{ZZT}\Big(\left(m_{\beta\alpha}^{\phi(0)} + m_{\beta\alpha}^{C(0)}\right)\ddot{u}_\beta^{(0)} + \left(m_{\beta\alpha}^{\phi(1)} + m_{\beta\alpha}^{C(1)}\right)\ddot{\theta}_\beta\\
&+\kappa_{ZZT}\left(m_{\beta\alpha}^{\phi\phi(0)} + m_{\beta\alpha}^{\phi C(0)} + m_{\beta\alpha}^{C\phi(0)} + m_{\beta\alpha}^{CC(0)}\right)\left(\ddot{\theta}_\beta + \ddot{u}_{3,\beta}^{(0)}\right)\Big)_{,\alpha}\delta u_3^{(0)}d\Omega\\
&+\kappa_{ZZT}\oint_\Gamma n_\alpha\Big(\left(m_{\beta\alpha}^{\phi(0)} + m_{\beta\alpha}^{C(0)}\right)\ddot{u}_\beta^{(0)} + \left(m_{\beta\alpha}^{\phi(1)} + m_{\beta\alpha}^{C(1)}\right)\ddot{\theta}_\beta\\
&+\left(m_{\beta\alpha}^{\phi\phi(0)} + m_{\beta\alpha}^{\phi C(0)} + m_{\beta\alpha}^{C\phi(0)} + m_{\beta\alpha}^{CC(0)}\right)\left(\ddot{\theta}_\beta + \ddot{u}_{3,\beta}^{(0)}\right)\Big)\delta u_3^{(0)}d\Gamma
\end{aligned} \tag{A37}$$

References

1. Jones, R.M. *Mechanics of Composite Materials*; CRC Press: Boca Raton, FL, USA, 1999; ISBN 978-1-315-27298-6.
2. Pagano, N.J. Exact Solutions for Composite Laminates in Cylindrical Bending. *J. Compos. Mater.* **1969**, *3*, 398–411. [CrossRef]
3. Pagano, N.J. Exact Solutions for Rectangular Bidirectional Composites and Sandwich Plates. *J. Compos. Mater.* **1970**, *4*, 20–34. [CrossRef]
4. Pagano, N.J. Influence of Shear Coupling in Cylindrical. Bending of Anisotropic Laminates. *J. Compos. Mater.* **1970**, *4*, 330–343. [CrossRef]
5. Srinivas, S.; Rao, A.K. Bending, Vibration and Buckling of Simply Supported Thick Orthotropic Rectangular Plates and Laminates. *Int. J. Solids Struct.* **1970**, *6*, 1463–1481. [CrossRef]
6. Srinivas, S.; Rao, A.K. A Three-Dimensional Solution for Plates and Laminates. *J. Frankl. Inst.* **1971**, *291*, 469–481. [CrossRef]
7. Savoia, M.; Reddy, J.N. A Variational Approach to Three-Dimensional Elasticity Solutions of Laminated Composite Plates. *J. Appl. Mech.* **1992**, *59*, S166–S175. [CrossRef]
8. Savoia, M.; Reddy, J.N. Three-Dimensional Thermal Analysis of Laminated Composite Plates. *Int. J. Solids Struct.* **1995**, *32*, 593–608. [CrossRef]

9. Noor, A.K.; Burton, W.S. Three-Dimensional Solutions for Antisymmetrically Laminated Anisotropic Plates. *J. Appl. Mech.* **1990**, *57*, 182–188. [CrossRef]
10. Noor, A.K.; Burton, W.S. Assessment of Computational Models for Multilayered Anisotropic Plates. *Compos. Struct.* **1990**, *14*, 233–265. [CrossRef]
11. Kashtalyan, M. Three-Dimensional Elasticity Solution for Bending of Functionally Graded Rectangular Plates. *Eur. J. Mech.-A/Solids* **2004**, *23*, 853–864. [CrossRef]
12. Brischetto, S. A General Exact Elastic Shell Solution for Bending Analysis of Functionally Graded Structures. *Compos. Struct.* **2017**, *175*, 70–85. [CrossRef]
13. Brischetto, S. Exact Three-Dimensional Static Analysis of Single- and Multi-Layered Plates and Shells. *Compos. Part B Eng.* **2017**, *119*, 230–252. [CrossRef]
14. Kirchhoff, G. Über das Gleichgewicht und die Bewegung Einer Elastischen Scheibe. *J. Für Die Reine Und Angew. Math. Crelles J.* **1850**, *1850*, 51–88. [CrossRef]
15. Reissner, E. The Effect of Transverse Shear Deformation on the Bending of Elastic Plates. *ASME J. Appl. Mech.* **1945**, *12*, A69–A77. [CrossRef]
16. Mindlin, R.D. Influence of Rotary Inertia and Shear on Flexural Motions of Isotropic, Elastic Plates. *J. Appl. Mech.* **1951**, *18*, 31–38. [CrossRef]
17. Reddy, J.N. A Simple Higher-Order Theory for Laminated Composite Plates. *J. Appl. Mech.* **1984**, *51*, 745–752. [CrossRef]
18. Abrate, S.; Di Sciuva, M. Equivalent Single Layer Theories for Composite and Sandwich Structures: A Review. *Compos. Struct.* **2017**, *179*, 482–494. [CrossRef]
19. Liew, K.M.; Pan, Z.Z.; Zhang, L.W. An Overview of Layerwise Theories for Composite Laminates and Structures: Development, Numerical Implementation and Application. *Compos. Struct.* **2019**, *216*, 240–259. [CrossRef]
20. Abrate, S.; Di Sciuva, M. Multilayer Models for Composite and Sandwich Structures. In *Comprehensive Composite Materials II*; Beaumont, P.W.R., Zweben, C.H., Eds.; Elsevier: Amsterdam, The Netherlands, 2018; pp. 399–425. ISBN 978-0-08-100534-7.
21. Di Sciuva, M. A Refinement of the Transverse Shear Deformation Theory for Multilayered Orthotropic Plates. In Proceedings of the AIDAA VII National Conference, Naples, Italy, 25 October 1983; Volume I, pp. 83–95.
22. Di Sciuva, M. Bending, Vibration and Buckling of Simply Supported Thick Multilayered Orthotropic Plates: An Evaluation of a New Displacement Model. *J. Sound. Vib.* **1986**, *105*, 425–442. [CrossRef]
23. Di Sciuva, M. Multilayered Anisotropic Plate Models with Continuous Interlaminar Stresses. *Compos. Struct.* **1992**, *22*, 149–167. [CrossRef]
24. Cho, M.; Parmerter, R.R. An Efficient Higher-Order Plate Theory for Laminated Composites. *Compos. Struct.* **1992**, *20*, 113–123. [CrossRef]
25. Cho, M.; Parmerter, R. Efficient Higher Order Composite Plate Theory for General Lamination Configurations. *AIAA J.* **1993**, *31*, 1299–1306. [CrossRef]
26. Icardi, U. Eight-Noded Zig-Zag Element for Deflection and Stress Analysis of Plates with General Lay-Up. *Compos. Part B Eng.* **1998**, *29*, 425–441. [CrossRef]
27. Icardi, U. Higher-Order Zig-Zag Model for Analysis of Thick Composite Beams with Inclusion of Transverse Normal Stress and Sublaminates Approximations. *Compos. Part B Eng.* **2001**, *32*, 343–354. [CrossRef]
28. Icardi, U. A Three-Dimensional Zig-Zag Theory for Analysis of Thick Laminated Beams. *Compos. Struct.* **2001**, *52*, 123–135. [CrossRef]
29. Tessler, A.; Di Sciuva, M.; Gherlone, M. Refinement of Timoshenko Beam Theory for Composite and Sandwich Beams Using Zigzag Kinematics. NASA/TP 2007-215086, 1 November 2007. pp. 1–45.
30. Averill, R.C. Static and Dynamic Response of Moderately Thick Laminated Beams with Damage. *Compos. Eng.* **1994**, *4*, 381–395. [CrossRef]
31. Averill, R.C.; Yip, Y.C. Development of Simple, Robust Finite Elements Based on Refined Theories for Thick Laminated Beams. *Comput. Struct.* **1996**, *59*, 529–546. [CrossRef]
32. Murakami, H. Laminated Composite Plate Theory With Improved In-Plane Responses. *J. Appl. Mech.* **1986**, *53*, 661–666. [CrossRef]
33. Tessler, A.; Di Sciuva, M.; Gherlone, M. Refined Zigzag Theory for Laminated Composite and Sandwich Plates. NASA/TP 2009-215561, 1 January 2009. pp. 1–53.
34. Sorrenti, M.; Di Sciuva, M. An Enhancement of the Warping Shear Functions of Refined Zigzag Theory. *J. Appl. Mech.* **2021**, *88*, 084501. [CrossRef]
35. Massabò, R.; Campi, F. An Efficient Approach for Multilayered Beams and Wide Plates with Imperfect Interfaces and Delaminations. *Compos. Struct.* **2014**, *116*, 311–324. [CrossRef]
36. Massabò, R.; Campi, F. Assessment and Correction of Theories for Multilayered Plates with Imperfect Interfaces. *Meccanica* **2015**, *50*, 1045–1071. [CrossRef]
37. Massabò, R.; Monetto, I. Modeling Imperfect Interfaces in Layered Beam through Multi- and Single-Variable Zigzag Kinematics. In Proceedings of the 8th European Congress on Computational Methods in Applied Sciences and Engineering, Oslo, Norway, 5 June 2022; p. 12.
38. Monetto, I.; Massabò, R. A Single-Variable Zigzag Approach to Model Imperfect Interfaces in Layered Beams. *Coatings* **2023**, *13*, 445. [CrossRef]

39. Nguyen, S.-N.; Lee, J.; Cho, M. Efficient Higher-Order Zig-Zag Theory for Viscoelastic Laminated Composite Plates. *Int. J. Solids Struct.* **2015**, *62*, 174–185. [CrossRef]
40. Nguyen, S.-N.; Lee, J.; Cho, M. A Triangular Finite Element Using Laplace Transform for Viscoelastic Laminated Composite Plates Based on Efficient Higher-Order Zigzag Theory. *Compos. Struct.* **2016**, *155*, 223–244. [CrossRef]
41. Dorduncu, M. Flexure Analysis of Functionally Graded Plates Using {2,2}-Refined Zigzag Theory. *J. Aeronaut. Space Technol.* **2019**, *12*, 19–30.
42. Ghorbanpour Arani, A.; Mosayyebi, M.; Kolahdouzan, F.; Kolahchi, R.; Jamali, M. Refined Zigzag Theory for Vibration Analysis of Viscoelastic Functionally Graded Carbon Nanotube Reinforced Composite Microplates Integrated with Piezoelectric Layers. *Proc. Inst. Mech. Eng. Part G. J. Aerosp. Eng.* **2017**, *231*, 2464–2478. [CrossRef]
43. Malekimoghadam, R.; Hosseini, S.A.; Icardi, U. Bending Analysis of Carbon Nanotube Coated–Fiber Multi-Scale Composite Beams Using the Refined Zigzag Theory. *Aerosp. Sci. Technol.* **2023**, *138*, 108328. [CrossRef]
44. Hajmohammad, M.H.; Nouri, A.H.; Zarei, M.S.; Kolahchi, R. A New Numerical Approach and Visco-Refined Zigzag Theory for Blast Analysis of Auxetic Honeycomb Plates Integrated by Multiphase Nanocomposite Facesheets in Hygrothermal Environment. *Eng. Comput.* **2019**, *35*, 1141–1157. [CrossRef]
45. Biswas, D.; Ray, C. Comparative Study on Transient Response Analysis of Hybrid Laminated Composite Plates with Experimental Verification. *J. Sound. Vib.* **2019**, *453*, 43–64. [CrossRef]
46. Groh, R.M.; Weaver, P.M.; Tessler, A. Application of the Refined Zigzag Theory to the Modeling of Delaminations in Laminated Composites. NASA/TM 2015-218808, 1 October 2015. pp. 1–22.
47. Eijo, A.; Oñate, E.; Oller, S. A Numerical Model of Delamination in Composite Laminated Beams Using the LRZ Beam Element Based on the Refined Zigzag Theory. *Compos. Struct.* **2013**, *104*, 270–280. [CrossRef]
48. Eijo, A.; Oñate, E.; Oller, S. Delamination in Laminated Plates Using the 4-Noded Quadrilateral QLRZ Plate Element Based on the Refined Zigzag Theory. *Compos. Struct.* **2014**, *108*, 456–471. [CrossRef]
49. Kefal, A.; Tessler, A. Delamination Damage Identification in Composite Shell Structures Based on Inverse Finite Element Method and Refined Zigzag Theory. In *Developments in the Analysis and Design of Marine Structures*; CRC Press: Boca Raton, FL, USA, 2021; pp. 354–363. ISBN 978-1-00-323037-3.
50. Ganjdoust, F.; Kefal, A.; Tessler, A. A Novel Delamination Damage Detection Strategy Based on Inverse Finite Element Method for Structural Health Monitoring of Composite Structures. *Mech. Syst. Signal Process.* **2023**, *192*, 110202. [CrossRef]
51. Shao, D.; Liang, W.; Wu, W.; Tao, Y. A Unified Transient Vibration Analysis of FGM Sandwich Plates in Thermal Environment Based on a Further Refined Zigzag Plate Theory. *Int. J. Struct. Stab. Dyn.* **2022**, *22*, 2250095. [CrossRef]
52. Wimmer, H.; Celigoj, C.; Hochhauser, W. A New Approach for Buckling Analysis of Laminated Glass Panels. *AIP Conf. Proc.* **2023**, *2928*, 150030. [CrossRef]
53. Ascione, A.; Orifici, A.C.; Gherlone, M. Experimental and Numerical Investigation of the Refined Zigzag Theory for Accurate Buckling Analysis of Highly Heterogeneous Sandwich Beams. *Int. J. Struct. Stab. Dyn.* **2020**, *20*, 2050078. [CrossRef]
54. Köpple, M.; Wagner, W. A Mixed Finite Element Model with Enhanced Zigzag Kinematics for the Non-Linear Analysis of Multilayer Plates. *Comput. Mech.* **2020**, *65*, 23–40. [CrossRef]
55. Ascione, A.; Gherlone, M.; Orifici, A.C. Nonlinear Static Analysis of Composite Beams with Piezoelectric Actuator Patches Using the Refined Zigzag Theory. *Compos. Struct.* **2022**, *282*, 115018. [CrossRef]
56. Flores, F.G. Implementation of the Refined Zigzag Theory in Shell Elements with Large Displacements and Rotations. *Compos. Struct.* **2014**, *118*, 560–570. [CrossRef]
57. Gherlone, M.; Versino, D.; Zarra, V. Multilayered Triangular and Quadrilateral Flat Shell Elements Based on the Refined Zigzag Theory. *Compos. Struct.* **2019**, *233*, 111629. [CrossRef]
58. Gao, Y.; Zhang, H.; Yang, W.; He, D. A New Bending Model for Composite Laminated Shells Based on the Refined Zigzag Theory. *Arch. Appl. Mech.* **2022**, *92*, 2899–2915. [CrossRef]
59. Kreja, I.; Sabik, A. Equivalent Single-Layer Models in Deformation Analysis of Laminated Multilayered Plates. *Acta Mech.* **2019**, *230*, 2827–2851. [CrossRef]
60. Sorrenti, M.; Gherlone, M.; Di Sciuva, M. Buckling Analysis of Angle-Ply Multilayered and Sandwich Plates Using the Enhanced Refined Zigzag Theory. *PEAS* **2022**, *71*, 84–102. [CrossRef]
61. Sorrenti, M.; Gherlone, M. A New Mixed Model Based on the Enhanced-Refined Zigzag Theory for the Analysis of Thick Multilayered Composite Plates. *Compos. Struct.* **2023**, *311*, 116787. [CrossRef]
62. Lewandowski, R.; Litewka, P.; Wielentejczyk, P. Free Vibrations of Laminate Plates with Viscoelastic Layers Using the Refined Zig-Zag Theory—Part 1. Theoretical Background. *Compos. Struct.* **2021**, *278*, 114547. [CrossRef]
63. Litewka, P.; Lewandowski, R.; Wielentejczyk, P. Free Vibrations of Laminate Plates with Viscoelastic Layers Using the Refined Zig-Zag Theory—Part 2. Numerical Analysis. *Compos. Struct.* **2021**, *278*, 114550. [CrossRef]
64. Dorduncu, M. Stress Analysis of Laminated Composite Beams Using Refined Zigzag Theory and Peridynamic Differential Operator. *Compos. Struct.* **2019**, *218*, 193–203. [CrossRef]
65. Dorduncu, M. Stress Analysis of Sandwich Plates with Functionally Graded Cores Using Peridynamic Differential Operator and Refined Zigzag Theory. *Thin Walled Struct.* **2020**, *146*, 106468. [CrossRef]
66. Honda, S.; Kumagai, T.; Tomihashi, K.; Narita, Y. Frequency Maximization of Laminated Sandwich Plates under General Boundary Conditions Using Layerwise Optimization Method with Refined Zigzag Theory. *J. Sound. Vib.* **2013**, *332*, 6451–6462. [CrossRef]

67. Hasim, K.A.; Kefal, A. Isogeometric Static Analysis of Laminated Plates with Curvilinear Fibers Based on Refined Zigzag Theory. *Compos. Struct.* **2021**, *256*, 113097. [CrossRef]
68. Kheyabani, A.; Ali, H.Q.; Kefal, A.; Yildiz, M. Coupling of Isogeometric Higher-Order RZT and Parametric HFGMC Frameworks for Multiscale Modeling of Sandwich Laminates: Theory and Experimental Validation. *Aerosp. Sci. Technol.* **2024**, *146*, 108944. [CrossRef]
69. Kefal, A.; Tessler, A.; Oterkus, E. An Enhanced Inverse Finite Element Method for Displacement and Stress Monitoring of Multilayered Composite and Sandwich Structures. *Compos. Struct.* **2017**, *179*, 514–540. [CrossRef]
70. Kefal, A.; Tabrizi, I.E.; Yildiz, M.; Tessler, A. A Smoothed iFEM Approach for Efficient Shape-Sensing Applications: Numerical and Experimental Validation on Composite Structures. *Mech. Syst. Signal Process.* **2021**, *152*, 107486. [CrossRef]
71. Abdollahzadeh, M.A.; Tabrizi, I.E.; Kefal, A.; Yildiz, M. A Combined Experimental/Numerical Study on Deformation Sensing of Sandwich Structures through Inverse Analysis of Pre-Extrapolated Strain Measurements. *Measurement* **2021**, *185*, 110031. [CrossRef]
72. Zhao, F.; Bao, H.; Liu, J.; Li, K. Shape Sensing of Multilayered Composite and Sandwich Beams Based on Refined Zigzag Theory and Inverse Finite Element Method. *Compos. Struct.* **2021**, *261*, 113321. [CrossRef]
73. Zhao, F. Real-Time Shape Sensing of Composite and Sandwich Structures by Coupling Inverse Finite-Element Method with Refined Zigzag Theory. *J. Eng. Mech.* **2023**, *149*, 04023070. [CrossRef]
74. Reddy, J.N. *Mechanics of Laminated Composite Plates and Shells: Theory and Analysis*, 2nd ed.; CRC Press: Boca Raton, FL, USA, 2003; ISBN 978-0-203-50280-8.
75. Di Sciuva, M. Geometrically Nonlinear Theory of Multilayered Plates with Interlayer Slips. *AIAA J.* **1997**, *35*, 1753–1759.
76. Gherlone, M.; Di Sciuva, M. Thermo-Mechanics of Undamaged and Damaged Multilayered Composite Plates: A Sub-Laminates Finite Element Approach. *Compos. Struct.* **2007**, *81*, 125–136. [CrossRef]
77. Kim, J.-S.; Cho, M. Enhanced Modeling of Laminated and Sandwich Plates via Strain Energy Transformation. *Compos. Sci. Technol.* **2006**, *66*, 1575–1587. [CrossRef]